

Exploring the advantages of multiband fMRI with simultaneous EEG to investigate coupling between gamma frequency neural activity and the BOLD response in humans

Uji, Makoto; Wilson, Ross; Francis, Susan; Mullinger, Karen; Mayhew, Stephen

DOI:
[10.1002/hbm.23943](https://doi.org/10.1002/hbm.23943)

License:
Other (please specify with Rights Statement)

Document Version
Peer reviewed version

Citation for published version (Harvard):
Uji, M, Wilson, R, Francis, S, Mullinger, K & Mayhew, S 2018, 'Exploring the advantages of multiband fMRI with simultaneous EEG to investigate coupling between gamma frequency neural activity and the BOLD response in humans', *Human Brain Mapping*, vol. 39, no. 4, pp. 1673-1687. <https://doi.org/10.1002/hbm.23943>

[Link to publication on Research at Birmingham portal](#)

Publisher Rights Statement:

This is the peer reviewed version of the following article: Uji M, Wilson R, Francis ST, Mullinger KJ, Mayhew SD. Exploring the advantages of multiband fMRI with simultaneous EEG to investigate coupling between gamma frequency neural activity and the BOLD response in humans. *Hum Brain Mapp.* 2018;39:1673–1687, which has been published in final form at: <https://doi.org/10.1002/hbm.23943>. This article may be used for non-commercial purposes in accordance with Wiley Terms and Conditions for Self-Archiving.

General rights

Unless a licence is specified above, all rights (including copyright and moral rights) in this document are retained by the authors and/or the copyright holders. The express permission of the copyright holder must be obtained for any use of this material other than for purposes permitted by law.

- Users may freely distribute the URL that is used to identify this publication.
- Users may download and/or print one copy of the publication from the University of Birmingham research portal for the purpose of private study or non-commercial research.
- User may use extracts from the document in line with the concept of 'fair dealing' under the Copyright, Designs and Patents Act 1988 (?)
- Users may not further distribute the material nor use it for the purposes of commercial gain.

Where a licence is displayed above, please note the terms and conditions of the licence govern your use of this document.

When citing, please reference the published version.

Take down policy

While the University of Birmingham exercises care and attention in making items available there are rare occasions when an item has been uploaded in error or has been deemed to be commercially or otherwise sensitive.

If you believe that this is the case for this document, please contact UBIRA@lists.bham.ac.uk providing details and we will remove access to the work immediately and investigate.



Exploring the advantages of multiband fMRI with simultaneous EEG to investigate coupling between gamma frequency neural activity and the BOLD response in humans.

Journal:	<i>Human Brain Mapping</i>
Manuscript ID	HBM-17-1128.R1
Wiley - Manuscript type:	Research Article
Date Submitted by the Author:	n/a
Complete List of Authors:	Uji, Makoto; School of Psychology and BUIC, University of Birmingham Wilson, Ross; School of Psychology and BUIC, University of Birmingham Francis, Susan; SPMIC, School of Physics and Astronomy, University of Nottingham Mullinger, Karen; SPMIC, School of Physics and Astronomy, University of Nottingham; School of Psychology and BUIC, University of Birmingham Mayhew, Stephen; School of Psychology and BUIC, University of Birmingham
Keywords:	EEG-fMRI, Multiband fMRI, Gamma-BOLD coupling, Gradient artefacts, Safety, Heating, Motor gamma oscillations, Multislice fMRI

SCHOLARONE™
Manuscripts

1
2
3 Exploring the advantages of multiband fMRI with simultaneous EEG to investigate coupling
4
5 between gamma frequency neural activity and the BOLD response in humans.
6
7

8
9 Makoto Uji^a, Ross Wilson^a, Susan T. Francis^b, Karen J. Mullinger^{a,b,*†}, Stephen D.
10
11 Mayhew^{a*}
12

13 ^a Centre for Human Brain Health (CHBH), School of Psychology, University of Birmingham,
14
15 Birmingham, UK
16

17 ^b Sir Peter Mansfield Imaging Centre (SPMIC), School of Physics and Astronomy, University
18
19 of Nottingham, Nottingham, UK
20
21

22 * these authors were equally responsible for leading this study
23

24 † corresponding author
25
26
27
28
29
30
31
32
33
34
35
36
37
38
39
40
41
42
43
44
45
46
47
48
49
50
51
52
53
54
55
56
57
58
59
60

Abstract

We established an optimal combination of EEG recording during sparse multiband (MB) fMRI that preserves high resolution, whole brain fMRI coverage whilst enabling broad-band EEG recordings which are uncorrupted by MRI gradient artefacts (GAs). We firstly determined the safety of simultaneous EEG recording during MB fMRI. Application of MB factor=4 produced $<1^{\circ}\text{C}$ peak heating of electrode/hardware during 20-minutes of GE-EPI data acquisition. However, higher SAR sequences require specific safety testing, with greater heating observed using PCASL with MB factor=4. Heating was greatest in the electrocardiogram channel, likely due to it possessing longest lead length. We investigated the effect of MB factor on the temporal signal to noise ratio for a range of GE-EPI sequences (varying MB factor and temporal interval between slice acquisitions). We found that, for our experimental purpose, the optimal acquisition was achieved with MB factor=3, 3mm isotropic voxels and 33 slices providing whole head coverage. This sequence afforded a 2.25s duration quiet period (without GAs) in every 3s TR. Using this sequence we demonstrated the ability to record gamma frequency (55-80Hz) EEG oscillations, in response to right index finger abduction, that are usually obscured by GAs during continuous fMRI data acquisition. In this novel application of EEG-MB fMRI to a motor task we observed a positive correlation between gamma and BOLD responses in bilateral motor regions. These findings support and extend previous work regarding coupling between neural and haemodynamic measures of brain activity in humans and showcase the utility of EEG-MB fMRI for future investigations.

Keywords

EEG-fMRI
Multiband or multislice fMRI
Gamma-BOLD coupling
Gradient artefacts
Safety
Heating
Motor gamma oscillations

Introduction

Electroencephalography (EEG) and functional magnetic resonance imaging (fMRI) are two neuroimaging techniques that are often used to investigate human brain function. Simultaneous EEG-fMRI recordings provide a wide range of complimentary information and can be advantageous for improving our understanding of brain function, for example: through investigating the spatiotemporal dynamics of neural activity (for a review, see Huster et al., 2012), or studying the underlying neurophysiological origins of the measured responses by comparing neural and haemodynamic signals e.g. (Mullinger et al., 2013). The primary advantage of simultaneous EEG-fMRI acquisition over separate recordings is that it enables investigation of unpredictable or spontaneous brain activity, as well as studying the trial-by-trial covariation in brain processing as measured by the two techniques (Bagshaw et al., 2004; Becker et al., 2011; Debener et al., 2006; Eichele et al., 2008; Goldman et al., 2002; Horovitz et al., 2008; Mayhew et al., 2013; Mobascher et al., 2009; Mullinger et al., 2014; Olbrich et al., 2009; Scheibe et al., 2010). Thus simultaneous recordings enable spatial localisation of temporally dynamic response features. EEG-fMRI analysis has provided many novel insights into brain function. For example, such analyses have demonstrated specific BOLD correlates of: distinct neurophysiological components including the auditory oddball (Bénar et al., 2007; Eichele et al., 2005) and the error-related negativity (Debener et al., 2005); as well as specific neural activity in specific frequency bands (Goldman et al., 2002; Laufs et al., 2003). These studies have shown that simultaneous EEG-fMRI can provide greater specificity regarding the spatial arrangement (Goldman et al., 2009; Novitskiy et al., 2011) or the temporal sequence (Eichele et al., 2005; Mayhew et al., 2012) of responsive brain areas, compared to that revealed by a standard analysis of data from a single neuroimaging modality.

Recently, neuronal activity in the gamma frequency band, which is typically defined as between approximately 30-100Hz, has attracted much interest because gamma

1
2
3 synchronization has been linked with a range of cognitive and sensory functions (Buschman
4 and Miller, 2007; Buzsaki and Draguhn, 2004; Colgin et al., 2009; Fries, 2009; Singer and
5 Gray, 1995). Gamma-band synchronization has been observed in humans using non-invasive
6 imaging methods during visual (Hoogenboom et al., 2006; Muthukumaraswamy and Singh,
7 2013), somatosensory (Bauer et al., 2006) and auditory (Pantev et al., 1991; Schadow et al.,
8 2009) stimulation. It is also known to be involved in higher cognitive functions such as
9 memory processes (Fell et al., 2001; Howard et al., 2003) and motor control (Brown et al.,
10 1998; Cheyne et al., 2008; Crone et al., 1998; Darvas et al., 2010; Gaetz et al., 2010;
11 Muthukumaraswamy, 2010; Schoffelen et al., 2005). Therefore, due to the functional
12 importance of gamma frequency activity, characterising the underlying mechanisms of these
13 responses is of great interest.

14
15
16
17
18
19
20
21
22
23
24
25
26
27 The majority of previous work investigating the link between BOLD signals and gamma
28 activity has been conducted using invasive electrode recordings of local-field potentials in
29 humans (Mukamel et al., 2005; Murta et al., 2016; Nir et al., 2007), primates (Logothetis et
30 al., 2001; Magri et al., 2012; Niessing et al., 2005; Scholvinck et al., 2010; Viswanathan and
31 Freeman, 2007) and rodents (Boorman et al., 2015; Sumiyoshi et al., 2012). These studies
32 showed the BOLD response is more strongly coupled to gamma frequency activity, compared
33 with the activity in the lower (<30Hz) frequency bands.

34
35
36
37
38
39
40
41
42
43 Whilst providing novel insights into neurovascular coupling, findings from invasive animal
44 recordings cannot be easily extrapolated to scalp electrophysiological recordings due to
45 differences in the recording references used and in the spatial scale of the neuronal
46 populations involved in generating the signals (Hall et al., 2005). In addition, although the
47 coupling between BOLD and gamma-LFP activity is widely cited as principle evidence for
48 the neural underpinnings of haemodynamic based functional neuroimaging, the majority of
49 these seminal studies have been conducted in visual cortex (Logothetis et al., 2001;
50
51
52
53
54
55
56
57
58
59
60

1
2
3 Viswanathan and Freeman, 2007), with some exceptions in auditory cortex (Mukamel et al.,
4 2005). A wider understanding in other brain regions, for example sensorimotor cortex, is
5 important to fully establish the fundamental nature of the gamma-BOLD relationship. Such
6 investigations are particularly important given the recent doubt cast on the functional
7 importance of narrow-band gamma responses in visual cortex (Hermes et al., 2014), and the
8 BOLD correlates of broader high-frequency activity (Winawer et al., 2013). Therefore non-
9 invasive simultaneous EEG-fMRI recordings in humans offer many potential advantages for
10 relating gamma and BOLD signals. Possibilities include extending previous studies
11 suggestions of a strong gamma-BOLD relationship by investigating this coupling in motor
12 paradigms, which have been widely shown to induce robust increases in gamma power
13 (Cheyne et al., 2008; Crone et al., 1998; Gaetz et al., 2010; Muthukumaraswamy, 2010), and
14 gaining a fuller understanding of the fundamental relationship of these signals to each other
15 and also to human behaviour (Hoogenboom et al., 2010; Womelsdorf et al., 2006).

16
17
18
19
20
21
22
23
24
25
26
27
28
29
30
31 However, few simultaneous EEG-fMRI studies have investigated gamma activity due to
32 technical limitations as detailed below, and consequently the relationship between
33 haemodynamic responses and the gamma band activity in humans remains incompletely
34 understood (Logothetis, 2008). The recording of EEG data in the MRI environment is
35 technically challenging primarily due to the effect of the MRI on the EEG data quality.
36
37
38
39
40
41
42
43
44
45
46
47
48
49
50
51
52
53
54
55
56
57
58
59
60
Namely, EEG data are corrupted by the gradient artefact (GA) produced by the time-varying
magnetic field gradients needed for imaging, the pulse artefact produced by cardiac pulse
driven motion in the strong magnetic field of the MR scanner, and motion artefacts due to
head movement in the MR environment (Mullinger and Bowtell, 2011). The frequency
characteristics of these artefacts mean that the GA is the primary problem for studying
gamma band activity, with residual GAs easily obscuring the small amplitude neuronal signal
of interest even after correction (Mullinger et al., 2011, 2008b).

1
2
3 Despite the technical challenges, a few studies have attempted to study the gamma band
4 using concurrent EEG and fMRI measures (Castelhano et al., 2014; Green et al., 2017; Leicht
5 et al., 2016; Mantini et al., 2007; Michels et al., 2010; Mulert et al., 2010; Rosa et al., 2010;
6 Scheeringa et al., 2011). Of these a number limited the frequency range of the measured
7 gamma band to a range of 30-50Hz (or narrower) to avoid the high frequencies where the
8 GAs dominate (e.g. Mantini et al., 2007; Mulert et al., 2010; Rosa et al., 2010). However, this
9 band limiting approach, is clearly suboptimal when gamma responses that are often reported
10 in the upper portion of the 30-100 Hz frequency range (Muthukumaraswamy, 2010) have
11 been related to behaviour and other neuronal measures e.g. GABA concentration
12 (Muthukumaraswamy et al., 2009). An alternative approach taken by other studies, or in
13 addition to band-limiting gamma, has been to adopt a sparse fMRI sequence (Leicht et al.,
14 2016; Mulert et al., 2010; Scheeringa et al., 2011) rather than conventional, continuous fMRI
15 acquisition. Sparse sequences feature an acquisition time shorter than the repetition time (TR)
16 of the MRI sequence in order to provide a time window with no MRI gradients present in
17 which to collect EEG data. As a result this approach enables the full gamma frequency range
18 to be investigated. However, conventional MRI sequences require a long TR (>3s) and/or
19 small number of slices to be acquired to provide the required sparsity; imposing limitations in
20 the temporal sampling or spatial coverage possible and consequently limiting the utility of the
21 fMRI data acquired.

22
23
24 Therefore in order to optimize simultaneous EEG-fMRI recordings to study gamma-BOLD
25 coupling, we need to establish a novel method to obtain cleaner EEG data in the high
26 (>30Hz) frequency band. Multiband (MB) fMRI has the potential to overcome the limitations
27 imposed by conventional sparse fMRI sequences. MB acquisition (Feinberg et al., 2010;
28 Moeller et al., 2010) can be employed to: shorten repetition times (TR); increase brain
29 coverage for a given TR; or shorten the acquisition time of whole-head fMRI in a sparse

1
2
3 fMRI sequence which would lengthen the gradient-free time window in which EEG data can
4 be collected. Sparse MB fMRI acquisitions therefore offer great potential for improving EEG
5 data quality during simultaneous acquisitions. However, due to the additional radio frequency
6 (RF) power of MB excitation the safety of EEG-MB fMRI acquisitions must be assessed
7 (Auerbach et al., 2013). In addition, as MB methods can affect temporal signal to noise
8 (tSNR) of fMRI data (Chen et al., 2015; Todd et al., 2016) assessing the implementation of
9 MB and the effect on fMRI tSNR is also important to enable optimised EEG-fMRI studies to
10 take place.

11
12 Therefore the aim of this work was to assess the overall feasibility of recording EEG
13 simultaneously with MB fMRI in humans. This took place in three parts: i) assessing the
14 safety implications of EEG-MB fMRI; ii) assessing the tSNR of MB fMRI and iii) applying
15 an optimised EEG-MB fMRI approach to investigate single-trial coupling relationships
16 between MB-BOLD and gamma and beta frequency EEG responses to a finger-abduction
17 motor task. We chose to investigate motor responses **as an event-related synchronisation**
18 **(ERS) of gamma oscillations (reflecting an increase in power), typically accompanied by**
19 **desynchronization (ERD) of beta frequency (15-30Hz) oscillations (reflecting a reduction in**
20 **power)**, in the primary motor cortex contralateral to the movement have been well
21 documented using invasive electroencephalography (ECoG) (Darvas et al., 2010), MEG
22 (Muthukumaraswamy, 2010) and EEG (Cheyne et al., 2008) (for reviews, Cheyne and
23 Ferrari, 2013; Cheyne, 2013; Muthukumaraswamy, 2013). To our knowledge, the motor
24 gamma-BOLD relationship has not previously been investigated with simultaneous EEG-
25 fMRI acquisition in humans. Therefore, through this proof of concept study we also aim to
26 widen the understanding of gamma-BOLD coupling across the cortex. We hypothesise that
27 the single-trial positive BOLD response in contralateral motor cortex will correlate positively
28 with **gamma power ERS and negatively with beta power ERD.**

Methods

Data were acquired and analysed in two stages. Stage one consisted of initial safety testing and image-quality optimisation of EEG-MB fMRI; whilst stage two involved the application of the optimised scanning protocol for the concurrent EEG-fMRI study of human brain responses during motor tasks.

During both stages, EEG data were acquired using BrainAmp MRplus EEG amplifiers (Brain Products, Munich) with 5kHz sampling rate and an MR-compatible 63-channel EEG cap (EasyCap, Herrsching). **The hardware band-pass filters were set to a 0.016-250 Hz range, with a roll-off of 30 dB/octave at high frequency.** Electrode layout followed the extended international 10-20 system with an additional channel for recording the electrocardiogram (ECG). FCz was used as the reference electrode. A 3T Philips Achieva MRI scanner with a body transmit and 32-channel receiver-array head coil was used for MR data acquisition. The MB implementation for fMRI acquisitions in this study was from Gyrotools, Zurich. MR-EEG scanner clocks were synchronised for all EEG data acquisition (Mullinger et al., 2008b). All data acquisition on humans was performed with approval from the local ethics committee and informed consent was obtained from all subjects involved in this project.

Stage 1: Assessing the safety and tSNR of EEG-MB fMRI

Safety testing

Safety testing was performed on a conductive, head shaped phantom with a conductivity of about $0.5\Omega^{-1}\text{m}^{-1}$ to mimic skin conductivity (Yan et al., 2010). The phantom was left in the scanner room over night to equilibrate to the ambient temperature. The EEG cap was then

1
2
3 connected to the phantom using conductive gel (Abralyte 2000 [EasyCap GmbH, Munich])
4
5 and all electrode impedances were maintained below 15k Ω . Fibre-optic thermometers
6
7 (Luxtron Corporation, Santa Clara, CA, USA) were used to continually monitor (1 Hz
8
9 sampling rate) heating effects at seven locations: four scalp electrodes (Cz, TP7, FCz & TP8),
10
11 the ECG lead (connected to the base of the phantom's neck), the cable bundle coming from
12
13 the EEG cap and the scanner bore (as a control measurement of heating effects unrelated to
14
15 the presence of the EEG system). Thermometer sensors were placed in the conductive gel
16
17 under the electrodes and taped to the surface of the cable bundle and scanner bore. The
18
19 phantom was then placed at the MR scanner iso-centre. Firstly, a 5-minute recording of
20
21 baseline temperature at each location was collected without any scanning. Then two 20-
22
23 minute MRI scans, both employing MB factor 4 and **spectral presaturation with inversion**
24
25 **recovery (SPIR)** fat suppression, were performed to test for heating during the highest
26
27 realistic values of specific absorption rate (SAR) for a given sequence type. **Please note MB**
28
29 **factor 4 was the highest available in this implementation of MB.** The sequences tested were:
30
31
32 1) gradient echo (GE)-EPI (using: TR/TE=1000/40ms, SENSE=2, slices=48, B1
33
34 RMS=1.09 μ T, SAR/head=22%); 2) Pseudo-continuous arterial spin labelling (PCASL)-GE-
35
36 EPI (using: TR/TE=3500/9.8ms, SENSE=2, slices=32, B1 RMS=1.58 μ T, SAR/head=46%).
37
38 Between the two MRI scans there was a 10 minute period without scanning to allow a return
39
40 to baseline following any heating effects from the previous MRI scan.
41
42
43

44 Analysis

45
46
47 The mean baseline temperature at each thermometer location was determined using the 5
48
49 minute recording prior to each MRI scan. For each location, the mean baseline temperature
50
51 was then subtracted from the temperature timeseries recorded during each scan to give the
52
53 change in temperature across the whole 20 minute scan period.
54
55
56
57
58
59
60

Image quality: tSNR

To assess the effect of the implementation of MB excitation on the fMRI signal tSNR, fMRI data were recorded on 3 healthy-adult subjects (age 32 ± 2 years) during five different GE-EPI pulse sequences:

- i) MB factor = 1 with equidistant slice acquisition
- ii) MB factor = 2 with equidistant slice acquisition
- iii) MB factor = 2 with sparse slice acquisition
- iv) MB factor = 3 with equidistant slice acquisition
- v) MB factor = 3 with sparse slice acquisition

Equidistant acquisition used the full TR period, comprised of equal temporal intervals between each slice acquisition. For sparse acquisitions MR data were acquired in the minimum possible time at the beginning of the TR period; the rest of the TR period then formed a quiet period with no MR gradients. A TR = 3060ms and 36 slices were chosen to ensure that these parameters could be used for all combinations of MB factors and slice acquisition (in scans i-v) whilst adhering to requirements for EEG clock synchronisation (Mandelkow et al., 2006; Mullinger et al., 2008b). Other parameters were set for all scans as follows: TE= 40ms, SENSE=2, flip angle=79°, 41 volumes acquired. A T1-weighted anatomical image was also acquired for each subject.

Analysis

For each subject the anatomical image was used to segment the grey matter (FSL FAST, <https://fsl.fmrib.ox.ac.uk/fsl/>) (Zhang et al., 2001) which formed a mask for subsequent analysis. The tSNR was calculated in every grey matter voxel (Eq. 1) and then averaged over voxels for each subject. The group mean and standard deviation in grey matter of the tSNR

was then found for each of the five scans to assess the change in tSNR with MB factor and slice acquisition scheme.

$$tSNR_{voxel} = \frac{\text{mean signal over time}_{voxel}}{\text{standard deviation over time}_{voxel}}$$

Eq. 1

Stage 2: EEG-fMRI motor study

12 right-handed subjects (10 males, 2 females, age = 26.6 ±5.7) took part in the study. After initial data processing, two subjects were excluded from further analysis due to repeated, excessive head motion (>4mm, as assessed from fMRI realignment parameters).

Data acquisition

The EEG cap was put on the subject and all electrode impedances were maintained below 10kΩ for the duration of the study. EEG-fMRI data were acquired using a sparse GE-EPI scheme (TR=3000ms (of which: acquisition time=750ms, quiet period=2250ms), TE=40ms, MB factor=3, 33 slices, voxels=3mm³, SENSE = 2, FOV = 240 x 240 mm, flip angle = 79°, 192 volumes, SAR/head<7%). These parameters had been optimised based on the results of Stage 1 and the requirements of the paradigm (see below). High frequency (>30 Hz) artefacts were minimised by mechanically isolating the EEG amplifiers from the scanner bed and minimising MR scanner room environment noise (Mullinger et al., 2013; Mullinger and Bowtell, 2011). In addition, the subject was positioned such that electrodes Fp1 and Fp2 were at the iso-centre in the foot/head direction so as to further reduce the amplitude of the GAs (Mullinger et al., 2011). Foam padding was placed around the subject's head to reduce motion-related artefacts. The EEG and MR scanner clocks were synchronised (**Brain Products Synchbox**), and the TR made equal to a multiple of the EEG sampling period, to ensure consistent sampling of the GA waveforms (Mandelkow et al., 2006; Mullinger et al.,

1
2
3 2008b). The onset of every TR period was marked in the EEG data to facilitate GA
4 correction. Simultaneous electromyogram (EMG) recordings were made from electrodes
5 attached over the first dorsal interosseous (FDI) muscle of the right hand using a Brain
6 Product EXG amplifier. Cardiac and respiratory cycles were simultaneously recorded using
7 the scanner's physiological monitoring system (vector cardiogram (VCG) and respiratory
8 belt). A T1-weighted anatomical image (MPRAGE sequence) with 1mm isotropic resolution
9 was also acquired. EEG electrode locations were digitised (Polhemus Fastrak) to facilitate
10 individualised co-registration of electrode positions with each subject's anatomical image.
11
12
13
14
15
16
17
18
19
20
21
22

23 *Paradigm*

24
25
26 Subjects performed abduction movements of the right-hand index finger in time with an
27 auditory cue (1 kHz tones, 50ms duration, 2.5Hz presentation rate) that was delivered to both
28 ears via headphones, as previously employed in an MEG study (Muthukumaraswamy, 2010).
29
30 A single trial consisted of four abduction movements which were performed briskly
31 following each auditory cue within the MR gradient quiet period of a single TR. The onset of
32 the first cue was 250ms after the end of the MR acquisition in that TR, such that the cues
33 occurred at 1000, 1400, 1800 and 2200ms relative to the start of a given TR, resulting in all
34 movements occurring within a 1.5s window for each trial. Abduction trials were separated by
35 a 16s (five 3s TR periods + 750ms MR acquisition + 250ms) resting baseline interval (see
36 Figure 1). Subjects were instructed to fixate on a centrally displayed cross, to keep their
37 hands by their sides and to remain as still as possible throughout the whole experiment.
38
39 Immediately prior to the first auditory cue of each trial, a visual cue appeared, the fixation
40 cross changed to a plus sign for 2s, warning the subjects to prepare for the upcoming trial.
41
42 Subjects performed a 10-minute practice outside the scanner (50 trials of the same auditory
43
44
45
46
47
48
49
50
51
52
53
54
55
56
57
58
59
60

1
2
3 **cued abduction task for 1.5s, separated by an interval of 5.5s and EEG recorded)** in order to
4 familiarize themselves with the paradigm and were then subsequently positioned inside the
5 MRI scanner where they each completed four runs of 30 trials during fMRI, resulting in 120
6 trials per subject in total.
7
8
9

10 11 Analysis

12 *EEG*

13
14
15 Cardiac R-peaks were detected from the VCG recording and used to inform pulse artefact
16 correction of data recording inside the scanner (Mullinger et al., 2008b). For both EEG and
17 EMG data, gradient and pulse artefacts were corrected in BrainVision Analyzer2 using
18 sliding window templates formed from the averages of 45 and 21 artefacts respectively,
19 which were subtracted from each occurrence of the respective artefacts. Data were
20 subsequently downsampled (600Hz), bandpass filtered (EEG: 0.5-120Hz, EMG: 0.5-45Hz)
21 and epoched into single-trials from -16s to 2s relative to the onset of the first auditory cue in
22 each trial (BrainVision Analyzer2). Through visual inspection of the data, noisy EEG
23 channels and trials that were contaminated with large motion artefacts, substantial EMG
24 activity during the baseline period, or showed a lack of abduction movement in the EMG
25 signal, were removed. This resulted in a group mean (\pm standard error [SE]) of 84 ± 2 trials
26 remaining for further analysis. Independent component analysis of the EEG data (ICA,
27 EEGLAB, <https://scn.ucsd.edu/eeglab/>) was then used to remove eye-blinks/movements
28 (Delorme and Makeig, 2004; Jung et al., 2000), with an average of 2 ICs ($SE = 1$) removed
29 per subject, and data were re-referenced to an average of all non-noisy channels.
30
31
32
33
34
35
36
37
38
39
40
41
42
43
44
45
46
47
48
49

50 Individual, 4-layer (scalp, skull, CSF, & brain) boundary element (BEM) head models were
51 constructed from the T1 anatomical image of each subject using the Fieldtrip toolbox
52 (<http://www.ru.nl/neuroimaging/fieldtrip>) (Oostenveld et al., 2011). A Linearly Constrained
53
54
55
56
57
58
59
60

1
2
3 Minimum Variance (LCMV) beamformer (Robinson and Vrba, 1999; van Dronkelen et al.,
4 1996; van Veen et al., 1997) was then employed to separately spatially localise changes in
5 each subject's gamma (55–80Hz) and beta (15-30Hz) frequency oscillations (filtered using
6
7 2nd order Butterworth filters implemented in Matlab) in response to abduction movements.
8
9
10 The optimal frequency band for the localisation of gamma ERS was determined based on an
11 iterative process of initially investigating time-frequency spectrograms created from broad
12 gamma band (30-100Hz) source localisation and observing that consistently, across subjects,
13 the peak gamma ERS was found in the 55-80Hz, gamma band range, in agreement with many
14 previous findings (Ball et al., 2008; Cheyne et al., 2008; Muthukumaraswamy, 2010; for
15 reviews, Cheyne and Ferrari, 2013; Cheyne, 2013; Muthukumaraswamy, 2013). For each
16 subject and frequency band (beta or gamma), source power during the active (0s to 1.5s) and
17 passive (-9.0s to -7.5s) time windows, defined relative to the first cue onset, were calculated.
18 The passive window definition in the baseline interval, during the first MR-quiet period that
19 preceded the visual probe cue of that trial, was chosen to avoid both the periods of MR
20 acquisition and any brain activity occurring due to the visual cue. Subsequently, pseudo T-
21 statistic (\mathbb{T} -statistic) maps were computed as the ratio of the difference in source power
22 between the active and passive windows, divided by the sum of the noise power estimates
23 inherent to the sensors during both active and passive windows (Hillebrand and Barnes, 2005;
24 Robinson and Vrba, 1999).

25
26
27
28
29
30
31
32
33
34
35
36
37
38
39
40
41
42
43
44 The maximum peak \mathbb{T} -statistic location of the gamma power ERS and minimum peak \mathbb{T} -
45 statistic location of the beta power ERD in the contralateral primary motor cortex (cM1)
46 defined the site of a gamma and a beta virtual electrode (VE). A broadband (1-120Hz)
47 timecourse of neural activity was then extracted from these two VE locations, by multiplying
48 the channel level data by the respective broadband beamformer weights. Time-frequency
49 spectrograms of gamma and beta VE data were calculated using a multitaper wavelet
50
51
52
53
54
55
56
57
58
59
60

1
2
3 approach (Scheeringa et al., 2011). Windows of 0.4s duration were moved across the data in
4
5 steps of 50ms, resulting in a frequency resolution of 2.5Hz, and the use of seven tapers
6
7 resulted in a spectral smoothing of ± 10 Hz. Using the mean of the passive window data as
8
9 baseline the spectrograms were converted to display change in activity relative to baseline.
10
11 Separately for each subject, VE timecourses were filtered into the gamma and beta bands,
12
13 Hilbert transformed and then the average power during the active window was calculated for
14
15 each trial (Mayhew et al., 2010; Mullinger et al., 2014). These single trial power values were
16
17 then mean-subtracted to form regressors of gamma and beta power, which represented the
18
19 trial-by-trial variability in single-trial stimulus response amplitudes, for subsequent GLM
20
21 analysis of fMRI data. The amplitude of rejected trials was set to the mean value (zero). EEG
22
23 data recorded outside the scanner were analysed using equivalent methodology, to provide
24
25 comparison of data quality with the inside scanner recordings.
26
27
28
29
30
31

32 *fMRI*

33
34
35 fMRI data were processed using FSL v5.0.9 (<https://fsl.fmrib.ox.ac.uk/fsl/>). Data from each
36
37 subject were corrected for physiological noise using a RETROICOR approach (Glover et al.,
38
39 1999) implemented using in-house Matlab code, motion corrected (MCFLIRT), spatially
40
41 smoothed (5mm FWHM Gaussian kernel), high-pass temporally filtered (100s cutoff),
42
43 registered to their T1 anatomical brain image (FLIRT), and normalised to the MNI 2mm
44
45 standard brain. GLM analyses were performed using FEAT v6.0. First-level analysis was
46
47 performed employing four regressors: 1) boxcar abduction movement, 2) boxcar visual probe
48
49 cue, 3&4) parametric modulation of single-trial gamma and beta neuronal responses,
50
51 respectively. All regressors were convolved with the double-gamma HRF. Both positive and
52
53 negative contrasts were assessed for each regressor. For each subject and frequency band,
54
55
56
57
58
59
60

1
2
3 first-level results were combined across all four runs using a second-level, fixed effects
4 analysis to calculate an average response per subject. These results were then combined
5 across all subjects at the third, group-level using a FLAME mixed-effects analysis (Woolrich
6 et al., 2004). Since our a-priori hypothesis was to investigate motor fMRI responses and their
7 correlation with gamma and beta EEG activity, a mask of motor cortex (Oxford–Harvard
8 cortical atlas, FSL) was applied as pre-threshold mask to all group-level statistical maps
9 before cluster correction. Main effect (boxcar model of the task) and the single trial EEG
10 regressor correlation BOLD Z-statistic images were threshold using $Z > 2.3$ and cluster
11 corrected significance threshold of $p < 0.05$.

22 23 24 25 **Results**

26 27 **Stage 1: Feasibility testing**

28 29 *Safety testing*

30
31
32
33
34 The temperature changes measured at all thermometer sensors during the GE-EPI sequence
35 are plotted in Figure 2. The greatest heating was observed in the ECG channel, which showed
36 a $\sim 0.5^{\circ}\text{C}$ increase. This temperature increase occurred gradually over the first 10 minutes and
37 then stabilised and showed no further change. Nominal heating was observed in the other
38 channels. The higher SAR of the PCASL sequence resulted in a greater heating effect than
39 the GE-EPI, again the largest temperature increase was seen in the ECG channel ($\sim 0.9^{\circ}\text{C}$)
40 with increases in other channels (TP8 = $\sim 0.8^{\circ}\text{C}$) also observed (Figure S1). As this GE-EPI
41 sequence, with parameters chosen to maximise SAR, showed no heating effect close to 1°C ,
42 the use of the MB GE-EPI (with parameters resulting in lower SAR) with the EEG system
43 was regarded safe for the following experiments (Carmichael et al., 2008; Medicines and
44 Healthcare Products Regulatory Agency, 2015).

Image quality: tSNR

The variation in BOLD tSNR with MB factor = 1-3 and slice spacing acquisition is summarised in Table 1. These data indicate that the variability in tSNR between subjects was far larger than the variability of tSNR with imaging parameters. Figure 3 shows the spatial variation in tSNR over a single slice for each subject for the two sparse imaging acquisition sequences tested, which were the most promising sequences for our EEG-fMRI application. Visual inspection of the images in Figure 3 and direct comparison of the mean and standard deviation of tSNR within subjects shows no clear change in tSNR ($12.6 \pm 22\%$ between MB factor 2 to 3) between MB factors. Since, for sparse sequences, using a MB factor of 3 compared with 2 results in a 33% reduction in the time required to acquire the same number of slices the MB factor of 3 was chosen for the EEG-fMRI experiment, to maximise the duration of the MR quiet-period for EEG measurements without degradation of the tSNR.

Study 2: EEG-fMRI motor study

All subjects performed the abduction task as instructed, judged by visual inspection of the EMG data showing increases in power during brisk finger movements which accurately timed to the auditory cues, and EMG power returning to rest levels during the baseline periods showing subjects remained still in these periods. Mean rectified EMG activity during the passive and active periods is shown for a representative subject in Figure 4.

Figure 5 shows the group average F -statistic map of changes in both EEG gamma- and beta-power during the active window compared to the passive window. An increase in gamma power (ERS, positive F values, Fig. 5a) was only observed in contralateral M1, whereas a decrease in beta power (ERD, negative F values, Fig. 5b) was observed in bilaterally in

1
2
3 contralateral and ipsilateral M1. Specifically, the mean of the individual subject VE locations
4 in cM1 for the gamma ERS was found at: $[-21\pm3, -31\pm3, 59\pm3]$ mm $[MNI:x,y,z]$ (see Fig 5a,
5 crosshair) and the beta ERD was found at $[-39\pm3, -32\pm2, 51\pm4]$ mm (see Fig 5b, crosshair),
6 where errors denote standard error over subjects. Both these locations lie in the post-central
7 gyrus, the gamma VE location was found to be significantly more medial ($t(9) = 3.76$,
8 $p=0.004$ paired t-test) than the beta VE location, but no difference in the y ($t(9) = 0.41$,
9 $p=0.69$) or z ($t(9) = 1.32$, $p=0.21$) co-ordinates was observed.
10
11
12
13
14
15
16
17

18 Figure 6 shows the group mean time-frequency spectrograms measured from cM1 for the
19 gamma (Fig 6a&b) and beta (Fig 6c&d) VE locations. Figures 6a&c display the mean time-
20 frequency spectrogram for the whole 18s duration of the abduction trial and preceding inter-
21 trial interval, with Figure 6b&d showing the active and passive periods only. The broadband
22 increases in power (red vertical stripes lasting ~ 750 ms and occurring every 3s) show the
23 effect of the residual GAs caused by the MRI data acquisition on the EEG power spectrum. It
24 is clear that neuronal EEG responses above 20 Hz recorded during MRI data acquisition are
25 corrupted by residual GAs with signal degradation increasing with increasing frequency (Fig.
26 6a&c). Note that, due to the way the trials were epoched, the increase in <30 Hz power
27 between -16s and -14s represents the post-movement alpha/beta rebound. By selecting the
28 active (0 to 1.5s) and passive (-9 to -7.5s) time windows during MR quiet periods a reliable
29 comparison of neuronal signals between rest and task was made for both the gamma and beta
30 bands (Fig. 6b&d). During the active window, when the FDI abduction movements were
31 performed, **ERS of gamma band power (55-80Hz) and ERD of beta band power (15-30Hz)**
32 occurred compared with the passive window of baseline resting fixation with no movement
33 (Fig. 6b&d). As expected due to the VE definition, stronger **gamma power ERS was observed**
34 **in the gamma VE than the beta VE, and stronger beta power ERD** was observed in the beta
35 VE than in the gamma VE. **Comparison of these results with those from data recorded outside**
36
37
38
39
40
41
42
43
44
45
46
47
48
49
50
51
52
53
54
55
56
57
58
59
60

1
2
3 the scanner (Figure S2 & S3), show that very similar gamma and beta responses were
4 measured in both recordings, providing confidence in the quality of our data inside the
5 scanner.
6
7
8
9

10 As expected across 10 subjects, we observed a significant main-effect (correlation with
11 boxcar regressor) positive BOLD response to the abduction movements in the motor cortex,
12 with the peak voxel ($Z=5.12$, $p<1\times 10^{-19}$) lying within the masked region found at $[-38, -32,$
13 $66]$ mm $[MNI:x,y,z]$ in cM1, as shown in Figure 7, red-orange. With a second peak ($Z=4.97$,
14 $p<1\times 10^{-19}$) found on the midline at $[-4, -14, 70]$ mm $[MNI:x,y,z]$. In addition a positive
15 correlation between single-trial gamma power ERS and the BOLD response was observed in
16 cM1, with the peak ($Z=3.11$, $p<0.001$) located at $[-32, -42, 60]$ mm $[MNI:x,y,z]$ (Fig 7, green)
17 with additional responses in the ipsilateral primary motor cortex with the peak ($Z=3.02$,
18 $p<0.01$) located at $[34, -42, 60]$ mm $[MNI:x,y,z]$ and on the midline with peak ($Z=2.97$,
19 $p<0.01$) located at $[2, -36, 56]$ mm $[MNI:x,y,z]$. No significant negative correlations were
20 observed with the boxcar or gamma band regressors. No significant positive or negative
21 correlations between single-trial beta and BOLD responses were observed.
22
23
24
25
26
27
28
29
30
31
32
33
34
35
36
37
38
39
40

41 Discussion

42 Here, through a series of experiments we show that, with the right safety precautions and
43 MRI sequence choice, it is safe to simultaneously acquire EEG data with MB fMRI data,
44 despite the higher peak RF power required for MB acquisitions compared with conventional
45 fMRI acquisitions. We also show that, for the implementation of MB used here, there is no
46 measurable degradation of the fMRI signal tSNR when moving to a sparse acquisition with a
47 MB factor of 3 compared with the conventional continuous equi-spacing acquisition with no
48 MB factor, allowing for the presence of physiological noise. We finally show the
49
50
51
52
53
54
55
56
57
58
59
60

1
2
3 considerable gains that can be achieved in using MB fMRI with concurrent EEG data
4 acquisition by studying gamma-BOLD coupling with a simple motor task. We were able to
5 reliably detect the gamma response to finger abductions within cM1 and found that this
6 response was positively correlated with the BOLD response in bilateral primary motor cortex
7 with activation extending directly posterior to the hand-knob area of the contralateral motor
8 cortex.
9
10
11
12
13
14
15
16
17
18

19 *Safety and signal quality considerations*

20
21 We show that for a GE-EPI sequence using a MB factor of 4 resulting in a B1 RMS=1.09 μ T,
22 SAR/head=22% that the maximum heating observed over a 20 minute period was \sim 0.5 $^{\circ}$ C
23 (Figure 2) which is considerably less than the recommended 1 $^{\circ}$ C safety limit (Medicines and
24 Healthcare Products Regulatory Agency, 2015). Furthermore the majority of this 0.5 $^{\circ}$ C
25 temperature increase was observed within the first 5-6 minutes of scanning after which the
26 temperature remained relatively constant suggesting that there is not a linear heating effect
27 over time. Therefore even if data were continuously acquired for a longer period, which is
28 uncommon in neuroimaging studies, the risk to the subject is unlikely to increase greatly. A
29 similar pattern of heating was observed for the PCASL sequence where the greatest heating
30 occurred in the first few minutes before a plateau was reached (Figure S1). However, this
31 heating effect was far greater, up to \sim 0.9 $^{\circ}$ C over the electrodes and locations measured,
32 reflecting the increased B1 power used in that sequence (B1 RMS=1.58 μ T, SAR/head=46%).
33 As this temperature rise was only just within the safe limit for human tissue (Medicines and
34 Healthcare Products Regulatory Agency, 2015) and given that not all locations on the
35 phantom were monitored, we would strongly suggest sequences such as MB-PCASL should
36 not be used with concurrent EEG recordings. **Although we didn't record temperature data**
37
38
39
40
41
42
43
44
45
46
47
48
49
50
51
52
53
54
55
56
57
58
59
60

1
2
3 from occipital electrodes due to practical limitations, we believe temperature increases at
4
5 T7/T8 are likely to approximate the O1/O2 electrodes, due to similar wire lengths. The
6
7 greatest heating effect in both GE-EPI and PCASL scans was observed in the ECG lead. This
8
9 lead is considerably longer than the other leads in the EEG cap, which probably resulted in
10
11 greater RF absorption in this lead (Mullinger et al., 2008a) causing the larger heating effect
12
13 observed here. Given the potential to use the VCG system, supplied by the MRI
14
15 manufacturer, to monitor the cardiac cycle (Mullinger et al., 2008b) it would be possible to
16
17 reduce the risk of heating effects by removing the ECG lead and electrode from the EEG
18
19 setup. However, given the increase in temperature (~ 0.8 °C) in the Tp8 electrode, which also
20
21 has a relatively long lead, the removal of the ECG lead alone is unlikely to ensure that high
22
23 SAR sequences can be run safely with EEG system present. These findings are in general
24
25 agreement with recent work that also considered safety implication of MB (Foged et al.,
26
27 2017). It is also important to note that minimal heating effects were observed at the MRI
28
29 scanner bore location suggesting that the MR scanning was not increasing the ambient
30
31 temperature of the bore. Therefore the observed electrode heating specifically arose from the
32
33 interaction between the EEG system and the RF slice excitation pulses. These data highlight
34
35 the potential dangers of using MB sequences for EEG-fMRI where high SAR values can arise
36
37 from the increased B1 (Collins and Wang, 2011) and the need for specific safety testing of
38
39 any sequences used. Since there are choices in how the RF pulses required for MB sequences
40
41 can be implemented, with varying effects on SAR (Feinberg and Setsompop, 2013; Norris et
42
43 al., 2011; Wong, 2012), it is important that MB implementations by different MR
44
45 manufactures and software providers are individually tested before being used in human
46
47 experiments.
48
49
50
51
52
53
54
55
56
57
58
59
60

1
2
3 It is known that the use of MB can reduce image quality and consequently degrade the
4 temporal stability of the signals acquired using EPI based sequences (Chen et al., 2015; Todd
5 et al., 2016). However, due to the ability of MB to shorten the TR, the increased temporal
6 sampling can result in increased signal sensitivity per unit time as well as enhanced t-
7 statistics of activation maps (Todd et al., 2016). MB fMRI has been shown to be useful in a
8 number of different applications since its conception only a few years ago, with the relative
9 gains in sampling rate and voxel size that it can provide offsetting any signal quality
10 degradation incurred (Boyacıoğlu et al., 2015; Feinberg et al., 2010; Moeller et al., 2010;
11 Olafsson et al., 2015). Indeed, our own investigations showed that the variation in tSNR over
12 subjects was far greater than the variation in tSNR between the sequences tested with
13 different MB factors and slice acquisition schemes (Table 1). This suggests that the tSNR
14 measures were dominated by physiological noise and anatomical variability rather than
15 imaging sequence differences. Even when changes in tSNR within subjects between MB 2
16 and 3 were considered there no clear reduction was seen with increasing MB factor (Figure 3)
17 in these data. By using MB factor = 3 with sparse slice acquisition we were able to maintain
18 whole-head coverage whilst obtaining a 2.25s MR quiet period, within our 3s TR, in which to
19 study EEG-BOLD coupling. Therefore the relative gain in quiet period time far outweighed
20 effects on tSNR which were encountered.
21
22
23
24
25
26
27
28
29
30
31
32
33
34
35
36
37
38
39
40
41
42
43
44

45 *Benefits of MB fMRI for the simultaneous recording of high frequency EEG signals*

46

47 The presence of residual GAs in EEG data at frequencies above 20 Hz shows the necessity of
48 an MR quiet period to provide the best SNR for studying beta and gamma band signals.
49 These residual artefacts are present despite strict adherence to best-current practice
50 acquisition and the implementation of hardware solutions (synchronisation (Mandelkow et
51
52
53
54
55
56
57
58
59
60

1
2
3 al., 2006; Mullinger et al., 2008) and optimal positioning (Mullinger et al., 2011)) and
4
5 beamforming post-processing (Brookes et al., 2009, 2008) which are all designed to minimise
6
7 the residual GAs. Whilst the magnitude of the residual GA appears to increase with
8
9 frequency (Figure 6), it is actually relatively constant across the frequency bands above 20
10
11 Hz (Figure S4c&d), but the relative contribution of the GA to the overall signal is increased
12
13 due to the decrease in the amplitude of the underlying neuronal activity at higher frequencies
14
15 resulting in Figure S4e&f. These residual artefacts are likely to be caused by sub-millimetre
16
17 movements of the subject's head during data acquisition causing small changes in the GA
18
19 profile, preventing perfect correction by template subtraction methods (Ritter et al., 2007;
20
21 Yan et al., 2009). Given that such small head movements cannot be eliminated during
22
23 acquisition and the current lack of a post-processing method to completely remove residual
24
25 GAs from the EEG data, despite considerable effort by a number of groups (Brookes et al.,
26
27 2008; Freyer et al., 2009; Maziero et al., 2016; Moosmann et al., 2009), the merit of an MR
28
29 quiet period, that enables the study of higher frequency neuronal activity unadulterated by
30
31 concurrent fMRI acquisition, is clear.
32
33
34
35
36
37
38

39 Indeed, using a sparse MR sequence incorporating quiet periods has previously been
40
41 implemented to allow the study of gamma band activity during fMRI (Leicht et al., 2016;
42
43 Mulert et al., 2010; Scheeringa et al., 2011). We have extended these previous works by
44
45 showing that beta and gamma band activity from motor cortex can be measured in the MRI
46
47 environment. We observed an ERS of gamma band power during the abduction movements
48
49 compared with rest (Figs 5a and 6a&b) localised to cM1, in close agreement with previous
50
51 MEG studies (Ball et al., 2008; Cheyne, 2013; Darvas et al., 2010; Muthukumaraswamy,
52
53 2010). This gamma band response was accompanied by a decrease (ERD) in beta band power
54
55 (Figs 5b and 6c&d) which was observed in bilateral M1, in agreement with previous studies
56
57
58
59
60

1
2
3 collected outside an MRI environment (Darvas et al., 2013; Jurkiewicz et al., 2006;
4 Muthukumaraswamy et al., 2010). Interestingly, previous invasive and non-invasive
5 electrophysiological recordings have shown that the gamma ERS is more spatially focal to
6 cM1 than the beta ERD (Darvas et al., 2013; Miller et al., 2007), which was also observed in
7 our data. In addition to the difference in the spatial localisation of the gamma/beta responses,
8 we also observed different temporal profiles between the spectral responses from these
9 locations. The gamma ERS covered a relatively large frequency range (~50-80Hz) and,
10 whilst it could be seen for the entire movement period, it was strongest at initial movement
11 onset (i.e. 0-0.5s Fig 6a). The beta ERD was found to be much stronger and was present
12 consistently throughout the entire movement period. Together these differences in spatial
13 location and temporal response profile suggest different neuronal populations are driving
14 these two responses, in line with previous findings (Darvas et al., 2010; Miller et al., 2007).
15
16
17
18
19
20
21
22
23
24
25
26
27
28
29
30
31

32 Given the considerable advantages of MRI for providing excellent spatial resolution of brain
33 activity (De Martino et al., 2015; Heidemann et al., 2012) it is highly desirable to take
34 advantage of this feature in the investigation of the origin of electrophysiological responses,
35 where non-invasive EEG/MEG recordings are limited. However, previous studies (Leicht et
36 al., 2016; Mulert et al., 2010; Scheeringa et al., 2011) have required considerable
37 compromise on spatial resolution (slice thickness ranging from 4-8mm with slice gaps of 0.4-
38 1mm) and/or brain coverage (between 35 and 120mm) to provide a sufficient quiet period to
39 TR ratio (ranging between 30-90% of time) and sampling rate of MRI responses (TRs
40 between 3 and 3.63s). With the current implementation of MB we have shown that these
41 trade-offs can be minimised such that 3 mm isotropic voxels, with no slice gap and 99 mm
42 brain coverage with a quiet period to TR ratio of 75%, can be achieved with a TR of 3s.
43
44
45
46
47
48
49
50
51
52
53
54
55
56
57
58
59
60

BOLD responses and coupling to EEG responses and future research possibilities

Exploiting the advantages of EEG-MB fMRI has allowed us to show the potential of this technique for non-invasively investigating brain function. We found that, out of all our regressors, the boxcar model of the finger abductions showed the strongest correlation with the BOLD response, with the largest activations arising in the contralateral postcentral gyrus (M1) [-38, -32, 66] mm, and supplementary motor area [-4, -14, 70] mm as well as bilateral S2. All of which are regions expected to be activated in a simple sensorimotor task. Interestingly the regions of gamma-BOLD correlation were smaller and more focal, with peak activity being observed between the postcentral gyrus and superior parietal lobule both in contralateral [-32,-42, 60] mm, ipsilateral [34, -42, 60] mm regions, and a central peak found between precentral and postcentral gyrus at [2, -36, 56] mm. The contralateral activation extends to directly posterior to the hand-knob area of the left sensorimotor cortex, further suggesting this was a localised, task specific response. The bilaterality of this correlation, given the gamma ERS was lateralised to the left cM1, appears surprising, but falls consistently within the bilateral somatosensory cortex and therefore is likely to arise due to the mutual correlation of BOLD signals between the contralateral and ipsilateral regions of the somatosensory network for this task.

It is unsurprising given the robust task employed that the BOLD response was well characterised by a simple boxcar model and that this showed the strongest activations in the motor network. However, single-trial variability in BOLD and gamma ERS response amplitudes were well coupled in the somatosensory network. This finding supports previous work showing a tight coupling of natural variability in BOLD and gamma responses in the visual system (Logothetis, 2003; Scheeringa et al., 2011) and extends these findings into the

1
2
3 sensorimotor modality. It is likely that the BOLD-gamma coupling was most evident in the
4
5 sensory network where the variability to the task was the greatest and therefore least
6
7 explained by the boxcar constant main effect. We hypothesize that a greater amount of
8
9 response variability was elicited in the somatosensory network than the motor cortex as the
10
11 subject's abduction movements showed such a high level of consistency in both timing and
12
13 amplitude (Fig 4), reflecting similar motor output. However, it is possible that the sensation
14
15 of finger movement, and thus the somatosensory input, may have varied depending on what
16
17 external surfaces were touched with the finger when subjects' arms were slightly cramped for
18
19 space inside the scanner. Whilst this cannot be proven with these data, it provides a basis for
20
21 further investigation.
22
23

24
25
26
27
28 The lack of significant correlation between the beta ERD and BOLD responses appears a
29
30 surprising result given previous reports of negative beta-BOLD correlations (Ritter et al.,
31
32 2009) and the clear beta band responses which we observed (Fig 5b). However, here we
33
34 considered the variability in the EEG response which explained variance in the BOLD data in
35
36 addition to that explained by a constant amplitude boxcar model. Further inspection of our
37
38 data with a fixed effects cluster corrected $Z > 2.0$ group analysis showed that beta-BOLD
39
40 correlations were observed in central and ipsilateral motor cortex, but these did not survive
41
42 mixed effects $Z > 2.3$. Therefore it seems that the effect size was too weak for the beta
43
44 correlation to arise in our data sample. Beta ERD is widely observed during preparation and
45
46 execution of movements (Engel and Fries, 2010; Ritter et al., 2009; Zaepffel et al., 2013),
47
48 however there is a sparsity of evidence directly linking parameters of the beta ERD amplitude
49
50 to the quality of motor performance, leaving much still to be understood concerning beta
51
52 oscillations precise functional role (Engel and Fries, 2010; Kilavik et al., 2013; Pogosyan et
53
54 al., 2009). Given the beta ERD has been considered to be a simple gating mechanism (Fry et
55
56
57
58
59
60

1
2
3 al., 2016; Stevenson et al., 2011) required to allow neuronal activity involved in task
4
5 execution to take place in other, typically higher, frequency bands it is conceivable that the
6
7 amplitude variability of the ERD is less related to the task performance and reflects more of a
8
9 binarised signal to permit the necessary activation.
10

11
12
13
14
15 In conclusion we show that EEG can be safely acquired concurrently with GE-EPI MB-fMRI
16
17 data and allows the investigation of neuronal and hemodynamic task responses with high
18
19 spatial, temporal and spectral resolution. We use a simple motor task in this work to show
20
21 that tight gamma-BOLD coupling is observed on an individual trial basis, agreeing with
22
23 previous invasive recordings in both animal and human visual/auditory cortex. In the future
24
25 such methodologies that allow detailed integration of a wide frequency range of neural
26
27 signals may be used to build a more complete understanding of pathways of feedforward and
28
29 feedback neural communication and of how such signals contribute to neurovascular
30
31 coupling mechanisms and the generation of the hemodynamic response.
32
33
34
35
36
37

38 **Acknowledgements**

39
40 We thank the Birmingham Nottingham Strategic Collaboration Fund for supporting this work
41
42 and MU and a University of Nottingham Anne McLaren Fellowship for funding KJM and a
43
44 University of Birmingham Fellowship for funding SDM.
45
46
47
48
49

50 **References**

51
52
53 Auerbach, E.J., Xu, J., Yacoub, E., Moeller, S., Ugurbil, K., 2013. Multiband accelerated
54
55 spin-echo echo planar imaging with reduced peak RF power using time-shifted RF
56
57
58
59
60

pulses. *Magn Reson Med* 69, 1261–1267. doi:10.1002/mrm.24719

Bagshaw, A.P., Aghakhani, Y., Bénar, C.G., Kobayashi, E., Hawco, C., Dubeau, F., Pike, G.B., Gotman, J., 2004. EEG-fMRI of focal epileptic spikes: Analysis with multiple haemodynamic functions and comparison with gadolinium-enhanced MR angiograms. *Hum. Brain Mapp.* 22, 179–192. doi:10.1002/hbm.20024

Ball, T., Demandt, E., Mutschler, I., Neitzel, E., Mehring, C., Vogt, K., Aertsen, A., Schulze-Bonhage, A., 2008. Movement related activity in the high gamma range of the human EEG. *Neuroimage* 41, 302–310. doi:10.1016/j.neuroimage.2008.02.032

Bauer, M., Oostenveld, R., Peeters, M., Fries, P., 2006. Tactile spatial attention enhances gamma-band activity in somatosensory cortex and reduces low-frequency activity in parieto-occipital areas. *J Neurosci* 26, 490–501. doi:10.1523/JNEUROSCI.5228-04.2006

Becker, R., Reinacher, M., Freyer, F., Villringer, A., Ritter, P., 2011. How Ongoing Neuronal Oscillations Account for Evoked fMRI Variability. *J. Neurosci.* 31, 11016–11027. doi:10.1523/jneurosci.0210-11.2011

Bénar, C.G., Schön, D., Grimault, S., Nazarian, B., Burle, B., Roth, M., Badier, J.M., Marquis, P., Liegeois-Chauvel, C., Anton, J.L., 2007. Single-trial analysis of oddball event-related potentials in simultaneous EEG-fMRI. *Hum. Brain Mapp.* 28, 602–613. doi:10.1002/hbm.20289

Boorman, L., Harris, S., Bruyns-Haylett, M., Kennerley, A., Zheng, Y., Martin, C., Jones, M., Redgrave, P., Berwick, J., 2015. Long-Latency Reductions in Gamma Power Predict Hemodynamic Changes That Underlie the Negative BOLD Signal. *J. Neurosci.* 35, 4641–4656. doi:10.1523/JNEUROSCI.2339-14.2015

- 1
2
3 Boyacıoğlu, R., Schulz, J., Koopmans, P.J., Barth, M., Norris, D.G., 2015. Improved
4
5 sensitivity and specificity for resting state and task fMRI with multiband multi-echo EPI
6
7 compared to multi-echo EPI at 7T. *Neuroimage* 119, 352–361.
8
9 doi:10.1016/j.neuroimage.2015.06.089
10
11
- 12 Brookes, M.J., Mullinger, K.J., Stevenson, C.M., Morris, P.G., Bowtell, R., 2008.
13
14 Simultaneous EEG source localisation and artifact rejection during concurrent fMRI by
15
16 means of spatial filtering. *Neuroimage* 40, 1090–1104.
17
18 doi:10.1016/j.neuroimage.2007.12.030
19
20
- 21 Brookes, M.J., Vrba, J., Mullinger, K.J., Geirsdottir, G.B., Yan, W.X., Stevenson, C.M.,
22
23 Bowtell, R., Morris, P.G., 2009. Source localisation in concurrent EEG/fMRI:
24
25 applications at 7T. *Neuroimage* 45, 440–452. doi:S1053-8119(08)01160-9 [pii]
26
27 10.1016/j.neuroimage.2008.10.047
28
29
- 30 Brown, P., Salenius, S., Rothwell, J.C., Hari, R., 1998. Cortical correlate of the piper rhythm
31
32 in humans. *J. Neurophysiol.* 80, 2911–2917.
33
34
- 35 Buschman, T.J., Miller, E.K., 2007. Top-down versus bottom-up control of attention in the
36
37 prefrontal and posterior parietal cortices. *Science* 315, 1860–1862.
38
39 doi:10.1126/science.1138071
40
41
- 42 Buzsaki, G., Draguhn, A., 2004. Neuronal Oscillations in Cortical Networks. *Science* (80-.).
43
44 304, 1926–1929. doi:10.1126/science.1099745
45
46
- 47 Carmichael, D.W., Thornton, J.S., Rodionov, R., Thornton, R., McEvoy, A., Allen, P.J.,
48
49 Lemieux, L., 2008. Safety of localizing epilepsy monitoring intracranial
50
51 electroencephalograph electrodes using MRI: Radiofrequency-induced heating. *J. Magn.*
52
53 *Reson. Imaging* 28, 1233–1244. doi:10.1002/jmri.21583
54
55
56
57
58
59
60

- 1
2
3 Castelhano, J., Duarte, I.C., Wibral, M., Rodriguez, E., Castelo-Branco, M., 2014. The dual
4
5 facet of gamma oscillations: Separate visual and decision making circuits as revealed by
6
7 simultaneous EEG/fMRI. *Hum. Brain Mapp.* 35, 5219–5235. doi:10.1002/hbm.22545
8
9
- 10 Chen, L., Vu, A.T., Xu, J., Moeller, S., Ugurbil, K., Yacoub, E., Feinberg, D.A., 2015.
11
12 Evaluation of highly accelerated simultaneous multi-slice EPI for fMRI. *Neuroimage*
13
14 104, 452–459. doi:10.1016/j.neuroimage.2014.10.027
15
16
- 17 Cheyne, D., Bells, S., Ferrari, P., Gaetz, W., Bostan, A.C., 2008. Self-paced movements
18
19 induce high-frequency gamma oscillations in primary motor cortex. *Neuroimage* 42,
20
21 332–342. doi:10.1016/j.neuroimage.2008.04.178
22
23
- 24 Cheyne, D., Ferrari, P., 2013. MEG studies of motor cortex gamma oscillations: evidence for
25
26 a gamma “fingerprint” in the brain? *Front. Hum. Neurosci.* 7, 1–7.
27
28 doi:10.3389/fnhum.2013.00575
29
30
- 31 Cheyne, D.O., 2013. MEG studies of sensorimotor rhythms: A review. *Exp. Neurol.*
32
33 doi:10.1016/j.expneurol.2012.08.030
34
35
- 36 Colgin, L.L., Denninger, T., Fyhn, M., Hafting, T., Bonnevie, T., Jensen, O., Moser, M.-B.,
37
38 Moser, E.I., 2009. Frequency of gamma oscillations routes flow of information in the
39
40 hippocampus. *Nature* 462, 353–357. doi:10.1038/nature08573
41
42
- 43 Collins, C.M., Wang, Z., 2011. Calculation of radiofrequency electromagnetic fields and their
44
45 effects in MRI of human subjects. *Magn. Reson. Med.* 65, 1470–1482.
46
47 doi:10.1002/mrm.22845
48
49
- 50 Crone, N.E., Miglioretti, D.L., Gordon, B., Lesser, R.P., 1998. Functional mapping of human
51
52 sensorimotor cortex with electrocorticographic spectral analysis II. Event-related
53
54 synchronization in the gamma band. *Brain* 121, 2301–2315.
55
56
57
58
59
60

1
2
3 doi:10.1093/brain/121.12.2301
4

5 Darvas, F., Rao, R.P.N., Murias, M., 2013. Localized high gamma motor oscillations respond
6 to perceived biologic motion. *J. Clin. Neurophysiol.* 30, 299–307.
7

8
9 doi:10.1097/WNP.0b013e3182872f40
10

11
12 Darvas, F., Scherer, R., Ojemann, J.G., Rao, R.P., Miller, K.J., Sorensen, L.B., 2010. High
13 gamma mapping using EEG. *Neuroimage* 49, 930–938.
14

15
16 doi:10.1016/j.neuroimage.2009.08.041
17

18
19 De Martino, F., Moerel, M., Xu, J., Van De Moortele, P.F., Ugurbil, K., Goebel, R., Yacoub,
20 E., Formisano, E., 2015. High-resolution mapping of myeloarchitecture in vivo:
21 Localization of auditory areas in the human brain. *Cereb. Cortex* 25, 3394–3405.
22

23
24 doi:10.1093/cercor/bhu150
25

26
27 Debener, S., Ullsperger, M., Siegel, M., Engel, A.K., 2006. Single-trial EEG-fMRI reveals
28 the dynamics of cognitive function. *Trends Cogn. Sci.* 10, 558–563.
29

30
31 doi:10.1016/j.tics.2006.09.010
32

33
34 Debener, S., Ullsperger, M., Siegel, M., Fiehler, K., von Cramon, D.Y., Engel, A.K., 2005.
35

36 Trial-by-trial coupling of concurrent electroencephalogram and functional magnetic
37 resonance imaging identifies the dynamics of performance monitoring. *J Neurosci* 25,
38

39
40 11730–11737. doi:10.1523/JNEUROSCI.3286-05.2005
41

42
43 Delorme, A., Makeig, S., 2004. EEGLAB: an open source toolbox for analysis of single-trial
44

45 EEG dynamics including independent component analysis. *J Neurosci Methods* 134, 9–
46
47 21. doi:10.1016/j.jneumeth.2003.10.009 S0165027003003479 [pii]
48

49
50 Eichele, T., Calhoun, V.D., Moosmann, M., Specht, K., Jongsma, M.L.A., Quiroga, R.Q.,
51

52
53 Nordby, H., Hugdahl, K., 2008. Unmixing concurrent EEG-fMRI with parallel
54

1
2
3 independent component analysis. *Int. J. Psychophysiol.* 67, 222–234.

4
5 doi:10.1016/j.ijpsycho.2007.04.010

6
7
8 Eichele, T., Specht, K., Moosmann, M., Jongsma, M.L.A., Quiroga, R.Q., Nordby, H.,
9
10 Hugdahl, K., 2005. Assessing the spatiotemporal evolution of neuronal activation with
11
12 single-trial event-related potentials and functional MRI. *Proc Natl Acad Sci U S A* 102,
13
14 17798–17803. doi:10.1073/pnas.0505508102

15
16
17 Engel, A.K., Fries, P., 2010. Beta-band oscillations-signalling the status quo? *Curr. Opin.*
18
19 *Neurobiol.* doi:10.1016/j.conb.2010.02.015

20
21
22 Feinberg, D.A., Moeller, S., Smith, S.M., Auerbach, E., Ramanna, S., Gunther, M., Glasser,
23
24 M.F., Miller, K.L., Ugurbil, K., Yacoub, E., 2010. Multiplexed echo planar imaging for
25
26 sub-second whole brain fMRI and fast diffusion imaging. *PLoS One* 5, e15710.
27
28 doi:10.1371/journal.pone.0015710

29
30
31 Feinberg, D.A., Setsompop, K., 2013. Ultra-fast MRI of the human brain with simultaneous
32
33 multi-slice imaging. *J. Magn. Reson.* doi:10.1016/j.jmr.2013.02.002

34
35
36 Fell, J., Klaver, P., Lehnertz, K., Grunwald, T., Schaller, C., Elger, C.E., Fernandez, G.,
37
38 2001. Human memory formation is accompanied by rhinal-hippocampal coupling and
39
40 decoupling. *Nat. Neurosci.* 4, 1259–1264. doi:10.1038/nn759

41
42
43 Foged, M.T., Lindberg, U., Vakamudi, K., Larsson, H.B.W., Pinborg, L.H., Kjær, T.W.,
44
45 Fabricius, M., Svarer, C., Ozenne, B., Thomsen, C., Beniczky, S., Paulson, O.B., Posse,
46
47 S., 2017. Safety and EEG data quality of concurrent high-density EEG and high-speed
48
49 fMRI at 3 Tesla. *PLoS One* 12. doi:10.1371/journal.pone.0178409

50
51
52 Freyer, F., Becker, R., Anami, K., Curio, G., Villringer, A., Ritter, P., 2009. Ultrahigh-
53
54 frequency EEG during fMRI: Pushing the limits of imaging-artifact correction.

1
2
3 Neuroimage 48, 94–108. doi:10.1016/j.neuroimage.2009.06.022
4

5 Fries, P., 2009. Neuronal gamma-band synchronization as a fundamental process in cortical
6 computation. *Annu Rev Neurosci* 32, 209–224.
7

8
9 doi:10.1146/annurev.neuro.051508.135603
10

11
12 Fry, A., Mullinger, K.J., O'Neill, G.C., Barratt, E.L., Morris, P.G., Bauer, M., Folland, J.P.,
13 Brookes, M.J., 2016. Modulation of post-movement beta rebound by contraction force
14 and rate of force development. *Hum. Brain Mapp.* 37, 2493–2511.
15
16

17
18 doi:10.1002/hbm.23189
19

20
21 Gaetz, W., MacDonald, M., Cheyne, D., Snead, O.C., 2010. Neuromagnetic imaging of
22 movement-related cortical oscillations in children and adults: Age predicts post-
23 movement beta rebound. *Neuroimage* 51, 792–807.
24
25

26
27 doi:10.1016/j.neuroimage.2010.01.077
28

29
30 Glover, G.H., Li, T.Q., Ress, D., 1999. Image-based method for retrospective correction of
31 physiological motion effects in fMRI: RETROICOR. *Magn Res Med* 44 (1) 162-167.
32
33

34
35 doi:10.1002/mrm.1522-2594(200007)44
36

37
38 Goldman, R.I., Stern, J.M., Engel Jerome, J., Cohen, M.S., 2002. Simultaneous EEG and
39 fMRI of the alpha rhythm. *Neuroreport* 13, 2487–2492.
40
41

42
43 doi:10.1097/01.wnr.0000047685.08940.d0
44

45 Goldman, R.I., Wei, C.Y., Philiastides, M.G., Gerson, A.D., Friedman, D., Brown, T.R.,
46 Sajda, P., 2009. Single-trial discrimination for integrating simultaneous EEG and fMRI:
47 identifying cortical areas contributing to trial-to-trial variability in the auditory oddball
48 task. *Neuroimage* 47, 136–147. doi:10.1016/j.neuroimage.2009.03.062
49
50
51
52

53
54 Green, J.J., Boehler, C.N., Roberts, K.C., Chen, L.-C., Krebs, R.M., Song, A.W., Woldorff,
55
56

1
2
3 M.G., 2017. Cortical and Subcortical Coordination of Visual Spatial Attention Revealed
4 by Simultaneous EEG–fMRI Recording. *J. Neurosci.* 37, 7803–7810.

5
6 doi:10.1523/JNEUROSCI.0326-17.2017
7

8
9
10 Hall, S.D., Holliday, I.E., Hillebrand, A., Singh, K.D., Furlong, P.L., Hadjipapas, A., Barnes,
11 G.R., 2005. The missing link: Analogous human and primate cortical gamma
12 oscillations. *Neuroimage* 26, 13–17. doi:10.1016/j.neuroimage.2005.01.009
13
14

15
16
17 Heidemann, R.M., Ivanov, D., Trampel, R., Fasano, F., Meyer, H., Pfeuffer, J., Turner, R.,
18
19 2012. Isotropic submillimeter fMRI in the human brain at 7 T: combining reduced field-
20 of-view imaging and partially parallel acquisitions. *Magn Reson Med* 68, 1506–1516.
21
22 doi:10.1002/mrm.24156
23
24

25
26 Hermes, D., Miller, K.J., Wandell, B. a, Winawer, J., 2014. Stimulus Dependence of Gamma
27 Oscillations in Human Visual Cortex. *Cereb. Cortex* 1–9. doi:10.1093/cercor/bhu091
28
29

30
31 Hillebrand, A., Barnes, G.R., 2005. Beamformer Analysis of MEG Data. *Int. Rev. Neurobiol.*
32
33 doi:10.1016/S0074-7742(05)68006-3
34
35

36
37 Hoogenboom, N., Schoffelen, J.M., Oostenveld, R., Fries, P., 2010. Visually induced
38 gamma-band activity predicts speed of change detection in humans. *Neuroimage* 51,
39 1162–1167. doi:10.1016/j.neuroimage.2010.03.041
40
41

42
43 Hoogenboom, N., Schoffelen, J.M., Oostenveld, R., Parkes, L.M., Fries, P., 2006. Localizing
44 human visual gamma-band activity in frequency, time and space. *Neuroimage* 29, 764–
45 773. doi:10.1016/j.neuroimage.2005.08.043
46
47
48

49
50 Horovitz, S.G., Fukunaga, M., De Zwart, J.A., Van Gelderen, P., Fulton, S.C., Balkin, T.J.,
51
52 Duyn, J.H., 2008. Low frequency BOLD fluctuations during resting wakefulness and
53 light sleep: A simultaneous EEG–fMRI study. *Hum. Brain Mapp.* 29, 671–682.
54
55
56

1
2
3 doi:10.1002/hbm.20428
4

5 Howard, M.W., Rizzuto, D.S., Caplan, J.B., Madsen, J.R., Lisman, J., Aschenbrenner-
6 Scheibe, R., Schulze-Bonhage, A., Kahana, M.J., 2003. Gamma Oscillations Correlate
7 with Working Memory Load in Humans. *Cereb. Cortex* 13, 1369–1374.
8
9
10
11
12 doi:10.1093/cercor/bhg084
13

14 Huster, R.J., Debener, S., Eichele, T., Herrmann, C.S., 2012. Methods for simultaneous EEG-
15 fMRI: an introductory review. *J Neurosci* 32, 6053–6060.
16
17
18
19 doi:10.1523/JNEUROSCI.0447-12.2012
20

21 Jung, T.P., Makeig, S., Westerfield, M., Townsend, J., Courchesne, E., Sejnowski, T.J., 2000.
22 Removal of eye activity artifacts from visual event-related potentials in normal and
23 clinical subjects. *Clin Neurophysiol* 111, 1745–1758. doi:S1388-2457(00)00386-2 [pii]
24
25
26
27

28 Jurkiewicz, M.T., Gaetz, W., Bostan, A.C., Cheyne, D., 2006. Post-movement beta rebound
29 is generated in motor cortex: Evidence from neuromagnetic recordings. *Neuroimage* 32,
30
31
32
33 1281–1289.
34

35
36 Kilavik, B.E., Zaepffel, M., Brovelli, A., MacKay, W.A., Riehle, A., 2013. The ups and
37
38
39
40
41
42
43
44
45
46
47
48
49
50
51
52
53
54
55
56
57
58
59
60
61
62
63
64
65
66
67
68
69
70
71
72
73
74
75
76
77
78
79
80
81
82
83
84
85
86
87
88
89
90
91
92
93
94
95
96
97
98
99
100
101
102
103
104
105
106
107
108
109
110
111
112
113
114
115
116
117
118
119
120
121
122
123
124
125
126
127
128
129
130
131
132
133
134
135
136
137
138
139
140
141
142
143
144
145
146
147
148
149
150
151
152
153
154
155
156
157
158
159
160
161
162
163
164
165
166
167
168
169
170
171
172
173
174
175
176
177
178
179
180
181
182
183
184
185
186
187
188
189
190
191
192
193
194
195
196
197
198
199
200
201
202
203
204
205
206
207
208
209
210
211
212
213
214
215
216
217
218
219
220
221
222
223
224
225
226
227
228
229
230
231
232
233
234
235
236
237
238
239
240
241
242
243
244
245
246
247
248
249
250
251
252
253
254
255
256
257
258
259
260
261
262
263
264
265
266
267
268
269
270
271
272
273
274
275
276
277
278
279
280
281
282
283
284
285
286
287
288
289
290
291
292
293
294
295
296
297
298
299
300
301
302
303
304
305
306
307
308
309
310
311
312
313
314
315
316
317
318
319
320
321
322
323
324
325
326
327
328
329
330
331
332
333
334
335
336
337
338
339
340
341
342
343
344
345
346
347
348
349
350
351
352
353
354
355
356
357
358
359
360
361
362
363
364
365
366
367
368
369
370
371
372
373
374
375
376
377
378
379
380
381
382
383
384
385
386
387
388
389
390
391
392
393
394
395
396
397
398
399
400
401
402
403
404
405
406
407
408
409
410
411
412
413
414
415
416
417
418
419
420
421
422
423
424
425
426
427
428
429
430
431
432
433
434
435
436
437
438
439
440
441
442
443
444
445
446
447
448
449
450
451
452
453
454
455
456
457
458
459
460
461
462
463
464
465
466
467
468
469
470
471
472
473
474
475
476
477
478
479
480
481
482
483
484
485
486
487
488
489
490
491
492
493
494
495
496
497
498
499
500
501
502
503
504
505
506
507
508
509
510
511
512
513
514
515
516
517
518
519
520
521
522
523
524
525
526
527
528
529
530
531
532
533
534
535
536
537
538
539
540
541
542
543
544
545
546
547
548
549
550
551
552
553
554
555
556
557
558
559
560
561
562
563
564
565
566
567
568
569
570
571
572
573
574
575
576
577
578
579
580
581
582
583
584
585
586
587
588
589
590
591
592
593
594
595
596
597
598
599
600
601
602
603
604
605
606
607
608
609
610
611
612
613
614
615
616
617
618
619
620
621
622
623
624
625
626
627
628
629
630
631
632
633
634
635
636
637
638
639
640
641
642
643
644
645
646
647
648
649
650
651
652
653
654
655
656
657
658
659
660
661
662
663
664
665
666
667
668
669
670
671
672
673
674
675
676
677
678
679
680
681
682
683
684
685
686
687
688
689
690
691
692
693
694
695
696
697
698
699
700
701
702
703
704
705
706
707
708
709
710
711
712
713
714
715
716
717
718
719
720
721
722
723
724
725
726
727
728
729
730
731
732
733
734
735
736
737
738
739
740
741
742
743
744
745
746
747
748
749
750
751
752
753
754
755
756
757
758
759
760
761
762
763
764
765
766
767
768
769
770
771
772
773
774
775
776
777
778
779
780
781
782
783
784
785
786
787
788
789
790
791
792
793
794
795
796
797
798
799
800
801
802
803
804
805
806
807
808
809
810
811
812
813
814
815
816
817
818
819
820
821
822
823
824
825
826
827
828
829
830
831
832
833
834
835
836
837
838
839
840
841
842
843
844
845
846
847
848
849
850
851
852
853
854
855
856
857
858
859
860
861
862
863
864
865
866
867
868
869
870
871
872
873
874
875
876
877
878
879
880
881
882
883
884
885
886
887
888
889
890
891
892
893
894
895
896
897
898
899
900
901
902
903
904
905
906
907
908
909
910
911
912
913
914
915
916
917
918
919
920
921
922
923
924
925
926
927
928
929
930
931
932
933
934
935
936
937
938
939
940
941
942
943
944
945
946
947
948
949
950
951
952
953
954
955
956
957
958
959
960
961
962
963
964
965
966
967
968
969
970
971
972
973
974
975
976
977
978
979
980
981
982
983
984
985
986
987
988
989
990
991
992
993
994
995
996
997
998
999
1000

Laufs, H., Kleinschmidt, A., Beyerle, A., Eger, E., Salek-Haddadi, A., Preibisch, C., Krakow,
K., 2003. EEG-correlated fMRI of human alpha activity. *Neuroimage* 19, 1463–1476.

Leicht, G., Vauth, S., Polomac, N., Andreou, C., Rauh, J., Mu??mann, M., Karow, A.,
Mulert, C., 2016. EEG-Informed fMRI Reveals a Disturbed Gamma-Band-Specific
Network in Subjects at High Risk for Psychosis. *Schizophr. Bull.* 42, 239–249.
doi:10.1093/schbul/sbv092

- 1
2
3 Logothetis, N.K., 2008. What we can do and what we cannot do with fMRI. *Nature* 453,
4 869–878. doi:10.1038/nature06976
5
6
7
8 Logothetis, N.K., 2003. The underpinnings of the BOLD functional magnetic resonance
9 imaging signal. *J Neurosci* 23, 3963–3971.
10
11
12
13 Logothetis, N.K., Pauls, J., Augath, M., Trinath, T., Oeltermann, A., 2001.
14 Neurophysiological investigation of the basis of the fMRI signal. *Nature* 412, 150–157.
15 doi:10.1038/35084005
16
17
18
19
20 Magri, C., Schridde, U., Murayama, Y., Panzeri, S., Logothetis, N.K., 2012. The amplitude
21 and timing of the BOLD signal reflects the relationship between local field potential
22 power at different frequencies. *J Neurosci* 32, 1395–1407. doi:32/4/1395 [pii]
23 10.1523/JNEUROSCI.3985-11.2012
24
25
26
27
28
29 Mandelkow, H., Halder, P., Boesiger, P., Brandeis, D., 2006. Synchronization facilitates
30 removal of MRI artefacts from concurrent EEG recordings and increases usable
31 bandwidth. *Neuroimage* 32, 1120–1126. doi:10.1016/j.neuroimage.2006.04.231
32
33
34
35
36
37
38
39
40
41
42
43
44
45
46
47
48
49
50
51
52
53
54
55
56
57
58
59
60
- Mantini, D., Perrucci, M.G., Del Gratta, C., Romani, G.L., Corbetta, M., 2007.
Electrophysiological signatures of resting state networks in the human brain. *Proc Natl
Acad Sci U S A* 104, 13170–13175. doi:10.1073/pnas.0700668104
- Mayhew, S.D., Dirckx, S.G., Niazy, R.K., Iannetti, G.D., Wise, R.G., 2010. EEG signatures
of auditory activity correlate with simultaneously recorded fMRI responses in humans.
Neuroimage 49, 849–864. doi:10.1016/j.neuroimage.2009.06.080
- Mayhew, S.D., Li, S., Kourtzi, Z., 2012. Learning acts on distinct processes for visual form
perception in the human brain. *J. Neurosci.* 32, 775–86. doi:10.1523/JNEUROSCI.2033-
11.2012

- 1
2
3 Mayhew, S.D., Ostwald, D., Porcaro, C., Bagshaw, A.P., 2013. Spontaneous EEG alpha
4
5 oscillation interacts with positive and negative BOLD responses in the visual-auditory
6
7 cortices and default-mode network. *Neuroimage* 76, 362–372.
8
9 doi:10.1016/j.neuroimage.2013.02.070
10
11
12 Maziero, D., Velasco, T.R., Hunt, N., Payne, E., Lemieux, L., Salmon, C.E.G., Carmichael,
13
14 D.W., 2016. Towards motion insensitive EEG-fMRI: Correcting motion-induced
15
16 voltages and gradient artefact instability in EEG using an fMRI prospective motion
17
18 correction (PMC) system. *Neuroimage* 138, 13–27.
19
20 doi:10.1016/j.neuroimage.2016.05.003
21
22
23 Medicines and Healthcare Products Regulatory Agency, 2015. Safety Guidelines for
24
25 Magnetic Resonance Imaging Equipment in Clinical Use.
26
27
28 Michels, L., Bucher, K., Lüchinger, R., Klaver, P., Martin, E., Jeanmonod, D., Brandeis, D.,
29
30 2010. Simultaneous EEG-fMRI during a working memory task: Modulations in low and
31
32 high frequency bands. *PLoS One* 5, 1–15. doi:10.1371/journal.pone.0010298
33
34
35 Miller, K.J., Leuthardt, E.C., Schalk, G., Rao, R.P.N., Anderson, N.R., Moran, D.W., Miller,
36
37 J.W., Ojemann, J.G., 2007. Spectral Changes in Cortical Surface Potentials during
38
39 Motor Movement. *J. Neurosci.* 27, 2424–2432. doi:10.1523/JNEUROSCI.3886-06.2007
40
41
42 Mobascher, A., Brinkmeyer, J., Warbrick, T., Musso, F., Wittsack, H.J., Saleh, A., Schnitzler,
43
44 A., Winterer, G., 2009. Laser-evoked potential P2 single-trial amplitudes covary with
45
46 the fMRI BOLD response in the medial pain system and interconnected subcortical
47
48 structures. *Neuroimage* 45, 917–926. doi:10.1016/j.neuroimage.2008.12.051
49
50
51
52 Moeller, S., Yacoub, E., Oelman, C.A., Auerbach, E., Strupp, J., Harel, N., Ugurbil, K., 2010.
53
54 Multiband multislice GE-EPI at 7 tesla, with 16-fold acceleration using partial parallel
55
56 imaging with application to high spatial and temporal whole-brain fMRI. *Magn Reson*
57
58
59
60

1
2
3 Med 63, 1144–1153. doi:10.1002/mrm.22361
4

5 Moosmann, M., Schönfelder, V.H., Specht, K., Scheeringa, R., Nordby, H., Hugdahl, K.,
6
7 2009. Realignment parameter-informed artefact correction for simultaneous EEG-fMRI
8
9 recordings. *Neuroimage* 45, 1144–1150. doi:10.1016/j.neuroimage.2009.01.024
10
11

12 Mukamel, R., Gelbard, H., Arieli, A., Hasson, U., Fried, I., Malach, R., 2005. Coupling
13
14 between neuronal firing, field potentials, and FMRI in human auditory cortex. *Science*
15
16 309, 951–954. doi:10.1126/science.1110913
17
18

19 Mulert, C., Leicht, G., Hepp, P., Kirsch, V., Karch, S., Pogarell, O., Reiser, M., Hegerl, U.,
20
21 Jäger, L., Moller, H.J., McCarley, R.W., 2010. Single-trial coupling of the gamma-band
22
23 response and the corresponding BOLD signal. *Neuroimage* 49, 2238–2247.
24
25 doi:10.1016/j.neuroimage.2009.10.058
26
27

28 Mullinger, K.J., Bowtell, R., 2011. Combining EEG and FMRI. *Methods Mol. Biol.* 711,
29
30 303–326.
31
32

33 Mullinger, K.J., Debener, S., Coxon, R., Bowtell, R., 2008a. Effects of simultaneous EEG
34
35 recording on MRI data quality at 1.5, 3 and 7 tesla. *Int. J. Psychophysiol.* 67, 178–188.
36
37 doi:10.1016/j.ijpsycho.2007.06.008
38
39

40 Mullinger, K.J., Mayhew, S.D., Bagshaw, A.P., Bowtell, R., Francis, S.T., 2014. Evidence
41
42 that the negative BOLD response is neuronal in origin: a simultaneous EEG-BOLD-
43
44 CBF study in humans. *Neuroimage* 94, 263–274.
45
46
47

48 Mullinger, K.J., Mayhew, S.D., Bagshaw, A.P., Bowtell, R., Francis, S.T., 2013.
49
50 Poststimulus undershoots in cerebral blood flow and BOLD fMRI responses are
51
52 modulated by poststimulus neuronal activity. *Proc Natl Acad Sci U S A* 110, 13636–
53
54 13641. doi:10.1073/pnas.1221287110
55
56
57

- 1
2
3 Mullinger, K.J., Morgan, P.S., Bowtell, R.W., 2008b. Improved artifact correction for
4
5 combined electroencephalography/functional MRI by means of synchronization and use
6
7 of vectorcardiogram recordings. *J Magn Reson Imaging* 27, 607–616.
8
9 doi:10.1002/jmri.21277
10
11
12 Mullinger, K.J., Yan, W.X., Bowtell, R., 2011. Reducing the gradient artefact in
13
14 simultaneous EEG-fMRI by adjusting the subject's axial position. *Neuroimage* 54,
15
16 1942–1950. doi:S1053-8119(10)01281-4 [pii] 10.1016/j.neuroimage.2010.09.079
17
18
19 Murta, T., Hu, L., Tierney, T.M., Chaudhary, U.J., Walker, M.C., Carmichael, D.W.,
20
21 Figueiredo, P., Lemieux, L., 2016. A study of the electro-haemodynamic coupling using
22
23 simultaneously acquired intracranial EEG and fMRI data in humans. *Neuroimage* 142,
24
25 371–380. doi:10.1016/j.neuroimage.2016.08.001
26
27
28 Muthukumaraswamy, S.D., 2013. High-frequency brain activity and muscle artifacts in
29
30 MEG/EEG: a review and recommendations. *Front. Hum. Neurosci.* 7, 1–11.
31
32 doi:10.3389/fnhum.2013.00138
33
34
35 Muthukumaraswamy, S.D., 2010. Functional Properties of Human Primary Motor Cortex
36
37 Gamma Oscillations. *J. Neurophysiol.* 104, 2873–2885. doi:10.1152/jn.00607.2010
38
39
40 Muthukumaraswamy, S.D., Edden, R.A.E., Jones, D.K., Swettenham, J.B., Singh, K.D.,
41
42 2009. Resting GABA concentration predicts peak gamma frequency and fMRI
43
44 amplitude in response to visual stimulation in humans. *Proc Natl Acad Sci U S A* 106,
45
46 8356–8361. doi:10.1073/pnas.0900728106
47
48
49 Muthukumaraswamy, S.D., Singh, K.D., 2013. Visual gamma oscillations: The effects of
50
51 stimulus type, visual field coverage and stimulus motion on MEG and EEG recordings.
52
53 *Neuroimage* 69, 223–230. doi:10.1016/j.neuroimage.2012.12.038
54
55
56
57
58
59
60

- 1
2
3 Muthukumaraswamy, S.D., Singh, K.D., Swettenham, J.B., Jones, D.K., 2010. Visual gamma
4 oscillations and evoked responses: variability, repeatability and structural MRI
5 correlates. *Neuroimage* 49, 3349–3357. doi:10.1016/j.neuroimage.2009.11.045
6
7
8
9
10 Niessing J, Ebisch B, Schmidt K, Niessing M, Singer W, Galuske R, 2005. Hemodynamic
11 Signals Correlate Tightly with Synchronized Gamma Oscillations. *Science* (80-.). 309,
12 948–951. doi:10.1126/science.1110948
13
14
15
16
17 Nir, Y., Fisch, L., Mukamel, R., Gelbard-Sagiv, H., Arieli, A., Fried, I., Malach, R., 2007.
18 Coupling between Neuronal Firing Rate, Gamma LFP, and BOLD fMRI Is Related to
19 Interneuronal Correlations. *Curr. Biol.* 17, 1275–1285. doi:10.1016/j.cub.2007.06.066
20
21
22
23
24 Norris, D.G., Koopmans, P.J., Boyacio??lu, R., Barth, M., 2011. Power independent of
25 number of slices (PINS) radiofrequency pulses for low-power simultaneous multislice
26 excitation. *Magn. Reson. Med.* 66, 1234–1240. doi:10.1002/mrm.23152
27
28
29
30
31 Novitskiy, N., Ramautar, J.R., Vanderperren, K., De Vos, M., Mennes, M., Mijovic, B.,
32 Vanrumste, B., Stiers, P., Van den Bergh, B., Lagae, L., Sunaert, S., Van Huffel, S.,
33 Wagemans, J., 2011. The BOLD correlates of the visual P1 and N1 in single-trial
34 analysis of simultaneous EEG-fMRI recordings during a spatial detection task.
35 *Neuroimage* 54, 824–835. doi:10.1016/j.neuroimage.2010.09.041
36
37
38
39
40
41
42
43 Olafsson, V., Kundu, P., Wong, E.C., Bandettini, P.A., Liu, T.T., 2015. Enhanced
44 identification of BOLD-like components with multi-echo simultaneous multi-slice
45 (MESMS) fMRI and multi-echo ICA. *Neuroimage*.
46
47
48
49
50
51
52 Olbrich, S., Mulert, C., Karch, S., Trenner, M., Leicht, G., Pogarell, O., Hegerl, U., 2009.
53 EEG-vigilance and BOLD effect during simultaneous EEG/fMRI measurement.
54
55
56
57
58
59
60

- 1
2
3 Oostenveld, R., Fries, P., Maris, E., Schoffelen, J.M., 2011. FieldTrip: Open source software
4 for advanced analysis of MEG, EEG, and invasive electrophysiological data. *Comput*
5 *Intell Neurosci* 2011, 156869. doi:10.1155/2011/156869
6
7
8
9
10 Pantev, C., Makeig, S., Hoke, M., Galambos, R., Hampson, S., Gallen, C., 1991. Human
11 auditory evoked gamma-band magnetic fields. *Proc. Natl. Acad. Sci. U. S. A.* 88, 8996–
12 9000. doi:10.1073/pnas.88.20.8996
13
14
15
16
17 Pogosyan, A., Gaynor, L.D., Eusebio, A., Brown, P., 2009. Boosting Cortical Activity at
18 Beta-Band Frequencies Slows Movement in Humans. *Curr. Biol.* 19, 1637–1641.
19 doi:10.1016/j.cub.2009.07.074
20
21
22
23
24 Ritter, P., Becker, R., Graefe, C., Villringer, A., 2007. Evaluating gradient artifact correction
25 of EEG data acquired simultaneously with fMRI. *Magn. Reson. Imaging* 25, 923–932.
26 doi:10.1016/j.mri.2007.03.005
27
28
29
30
31 Ritter, P., Moosmann, M., Villringer, A., 2009. Rolandic alpha and beta EEG rhythms'
32 strengths are inversely related to fMRI-BOLD signal in primary somatosensory and
33 motor cortex. *Hum Brain Mapp* 30, 1168–1187. doi:10.1002/hbm.20585
34
35
36
37
38 Robinson, S.E., Vrba, J., 1999. Functional neuroimaging by synthetic aperture magnetometry
39 (SAM). *Recent Adv. Biomagn. Tohoku Uni*, 302–305.
40
41
42
43 Rosa, M.J., Kilner, J., Blankenburg, F., Josephs, O., Penny, W., 2010. Estimating the transfer
44 function from neuronal activity to BOLD using simultaneous EEG-fMRI. *Neuroimage*
45 49, 1496–1509. doi:10.1016/j.neuroimage.2009.09.011
46
47
48
49
50 Schadow, J., Lenz, D., Dettler, N., Fründ, I., Herrmann, C.S., 2009. NeuroImage Early
51 gamma-band responses reflect anticipatory top-down modulation in the auditory
52 cortex. *Neuroimage* 47, 651–658. doi:10.1016/j.neuroimage.2009.04.074
53
54
55
56
57
58
59
60

- 1
2
3 Scheeringa, R., Fries, P., Petersson, K.-M., Oostenveld, R., Grothe, I., Norris, D.G., Hagoort,
4
5 P., Bastiaansen, M.C.M., 2011. Neuronal Dynamics Underlying High- and Low-
6
7 Frequency EEG Oscillations Contribute Independently to the Human BOLD Signal.
8
9 *Neuron* 69, 572–583. doi:10.1016/j.neuron.2010.11.044
10
11
12 Scheibe, C., Ullsperger, M., Sommer, W., Heekeren, H.R., 2010. Effects of parametrical and
13
14 trial-to-trial variation in prior probability processing revealed by simultaneous
15
16 electroencephalogram/functional magnetic resonance imaging. *J Neurosci* 30, 16709–
17
18 16717. doi:10.1523/JNEUROSCI.3949-09.2010
19
20
21 Schoffelen, J., Oostenveld, R., Fries, P., 2005. Neuronal coherence as a mechanism of
22
23 effective corticospinal interaction. *Science* 308, 111–113. doi:10.1126/science.1107027
24
25
26 Scholvinck, M.L., Maier, A., Ye, F.Q., Duyn, J.H., Leopold, D.A., 2010. Neural basis of
27
28 global resting-state fMRI activity. *Proc Natl Acad Sci U S A* 107, 10238–10243.
29
30 doi:10.1073/pnas.0913110107 [pii] 10.1073/pnas.0913110107
31
32
33 Singer, W., Gray, C.M., 1995. Visual Feature Integration and the Temporal Correlation
34
35 Hypothesis. *Annu. Rev. Neurosci.* 18, 555–586. doi:10.1146/annurev.neuro.18.1.555
36
37
38 Stevenson, C.M., Brookes, M.J., Morris, P.G., 2011. β -Band correlates of the fMRI BOLD
39
40 response. *Hum. Brain Mapp.* 32, 182–197. doi:10.1002/hbm.21016
41
42
43 Sumiyoshi, A., Suzuki, H., Ogawa, T., Riera, J.J., Shimokawa, H., Kawashima, R., 2012.
44
45 Coupling between gamma oscillation and fMRI signal in the rat somatosensory cortex:
46
47 Its dependence on systemic physiological parameters. *Neuroimage* 60, 738–746.
48
49 doi:10.1016/j.neuroimage.2011.12.082
50
51
52 Todd, N., Moeller, S., Auerbach, E.J., Yacoub, E., Flandin, G., Weiskopf, N., 2016.
53
54 Evaluation of 2D multiband EPI imaging for high-resolution, whole-brain, task-based
55
56
57
58
59
60

- 1
2
3 fMRI studies at 3T: Sensitivity and slice leakage artifacts. *Neuroimage* 124, 32–42.
4
5 doi:10.1016/j.neuroimage.2015.08.056
6
7
8 van Drongelen, W., Yuchtman, M., Van Veen, B., van Huffelen, A., 1996. A spatial filtering
9
10 technique to detect and localize multiple sources in the brain. *Brain Topogr.* 9, 39–49.
11
12
13 van Veen, B.D., van Drongelen, W., Yuchtman, M., Suzuki, A., 1997. Localization of brain
14
15 electrical activity via linearly constrained minimum variance spatial filtering.
16
17 *Biomedical* 44, 867–880. doi:10.1109/10.623056
18
19
20 Viswanathan, A., Freeman, R.D., 2007. Neurometabolic coupling in cerebral cortex reflects
21
22 synaptic more than spiking activity. *Nat Neurosci* 10, 1308–1312. doi:10.1038/nn1977
23
24
25 Winawer, J., Kay, K.N., Foster, B.L., Rauschecker, A.M., Parvizi, J., Wandell, B.A., 2013.
26
27 Asynchronous Broadband Signals Are the Principal Source of the BOLD Response in
28
29 Human Visual Cortex. *Curr. Biol.* 23, 1145–1153. doi:10.1016/j.cub.2013.05.001
30
31
32 Womelsdorf, T., Fries, P., Mitra, P.P., Desimone, R., 2006. Gamma-band synchronization in
33
34 visual cortex predicts speed of change detection. *Nature* 439, 733–736.
35
36 doi:10.1038/nature04258
37
38
39 Wong, E., 2012. Optimized phase schedules for minimizing peak RF power in simultaneous
40
41 multi-slice RF excitation pulses, in: *Proceedings of the 20th Annual Meeting of*
42
43 *ISMRM.* Melbourne, Australia, p. 2209.
44
45
46 Woolrich, M.W., Behrens, T.E., Beckmann, C.F., Jenkinson, M., Smith, S.M., 2004.
47
48 Multilevel linear modelling for fMRI group analysis using Bayesian inference.
49
50 *Neuroimage* 21, 1732–1747. doi:10.1016/j.neuroimage.2003.12.023
51
52 S1053811903007894 [pii]
53
54
55 Yan, W.X., Mullinger, K.J., Brookes, M.J., Bowtell, R., 2009. Understanding gradient
56
57
58
59
60

1
2
3 artefacts in simultaneous EEG/fMRI. *Neuroimage* 46, 459–471.
4

5 Yan, W.X., Mullinger, K.J., Geirsdottir, G.B., Bowtell, R., 2010. Physical modeling of pulse
6 artefact sources in simultaneous EEG/fMRI. *Hum Brain Mapp* 31, 604–620.
7
8
9
10 doi:10.1002/hbm.20891
11

12 Zaepffel, M., Trachel, R., Kilavik, B.E., Brochier, T., 2013. Modulations of EEG Beta Power
13 during Planning and Execution of Grasping Movements. *PLoS One* 8, 1–10.
14
15
16
17 doi:10.1371/journal.pone.0060060
18

19 Zhang, Y., Brady, M., Smith, S., 2001. Segmentation of brain MR images through a hidden
20 Markov random field model and the expectation-maximization algorithm. *IEEE Trans*
21
22
23
24
25
26
27
28
29
30
31
32
33
34
35
36
37
38
39
40
41
42
43
44
45
46
47
48
49
50
51
52
53
54
55
56
57
58
59
60
Med Imaging 20, 45–57. doi:10.1109/42.906424

Figure Captions

Figure 1. Schematic of the sparse MB=3 fMRI scanning scheme and the motor task paradigm showing when four abduction movements were performed within the MR gradient quiet period of a single volume, and were followed by a 16s resting baseline interval for each trial. This results in the movements being performed every 18s.

Figure 2. Temperature changes at EEG electrodes, cable bundle and a control location on the scanner bore during a 20-minute GE-EPI sequence scan (MB factor = 4, TR/TE=1000/40ms, SENSE=2, slices=48, B1 RMS=1.09 μ T, SAR/head=22%) using a Philips Achieva 3T MRI scanner. Temperature was calculated relative to an initial 5-minute baseline recording made before the scan started.

Figure 3. Spatial maps of tSNR of middle slice of the stack for each subject for sparse image acquisition sequences with MB factor 2 (top row) and 3 (bottom row). The values below the each map show the mean tSNR \pm SD over all grey matter voxels for a given subject and scan.

Figure 4. EMG activity recorded from the right FDI during the passive (-9 to -7.5s) and active (0-1.5s) time windows (here the time windows are concatenated together for visualisation purposes) from three representative subjects. The average timecourse across all trials and runs from a representative subject is shown. Onset of the first auditory cue occurred at 0s relative to index finger abduction movements. Error bars denote standard deviation across runs.

Figure 5. Group average (N=10) F -statistic beamformer maps showing regions exhibiting power increases and decreases in **a)** gamma- and **b)** beta-power, respectively, during the active window (0-1.5s) as compared with the passive window (-9.5-7s). The crosshairs represent the group average of the individual VE locations found in cM1 for the gamma (**a)** and beta (**b)** frequency activity.

1
2
3 **Figure 6.** Group mean (N=10) time-frequency spectrograms demonstrating changes in the
4 EEG signal power in cM1 relative to the passive window (-9 to -7.5s) for **a&b)** gamma ERS
5 and **c&d)** beta ERD VE location. The passive window was located in an MR quiet period and
6 before any anticipation of the stimulus. Time is displayed relative to the auditory cue onset.
7 Spectrograms were calculated with frequency resolution of 2.5Hz with spectral smoothing of
8 ± 10 Hz. **a&c)** show 18s whole-trial duration, note the residual GAs during fMRI acquisition
9 periods. **b&d)** show the gamma and beta power responses during the active window (0 to
10 1.5s) where movement occurred, with the passive window data appended pre-stimulus for
11 comparison. Colour bars denote the relative change in power from the average power during
12 the passive window period (baseline measure) of the passive window for each frequency. See
13 Figure S4 for absolute power changes of same time-frequency spectrograms.
14
15
16
17
18
19
20
21
22
23
24
25
26

27 **Figure 7.** Group average (N=10) fMRI mixed effects results. Positive correlation of BOLD
28 signal to the boxcar model of right index finger abduction movements (red-yellow) and areas
29 of positive gamma-BOLD correlation (green). All correlations are cluster corrected with $p <$
30 0.05, masked with motor cortex. The crosshairs represent the peak positive gamma-BOLD
31 correlation in cM1 (at [-32, -42, 60] mm).
32
33
34
35
36
37
38
39
40
41
42
43
44
45
46
47
48
49
50
51
52
53
54
55
56
57
58
59
60

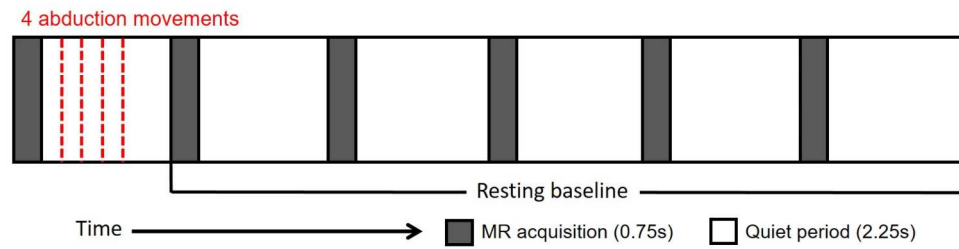


Figure 1: Schematic of the sparse MB=3 fMRI scanning scheme and the motor task paradigm showing when four abduction movements were performed within the MR gradient quiet period of a single volume, and were followed by a 16s resting baseline interval for each trial. This results in the movements being performed every 18s.

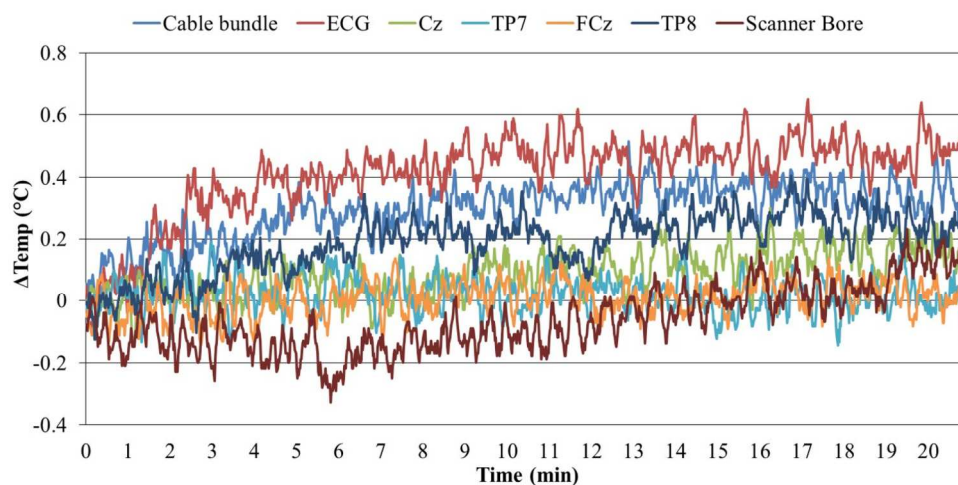


Figure 2: Temperature changes at EEG electrodes, cable bundle and a control location on the scanner bore during a 20-minute GE-EPI sequence scan (MB factor = 4, TR/TE=1000/40ms, SENSE=2, slices=48, B1 RMS=1.09 μT , SAR/head=22%) using a Philips Achieva 3T MRI scanner. Temperature was calculated relative to an initial 5-minute baseline recording made before the scan started.

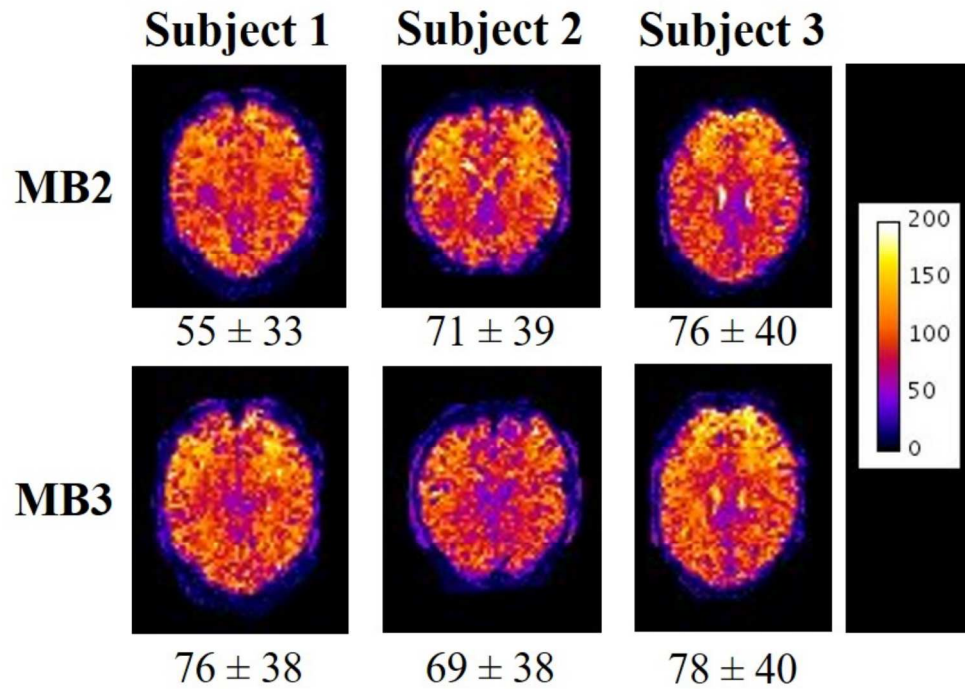


Figure 3: Spatial maps of tSNR of middle slice of the stack for each subject for sparse image acquisition sequences with MB factor 2 (top row) and 3 (bottom row). The values below the each map show the mean tSNR \pm SD over all grey matter voxels for a given subject and scan.

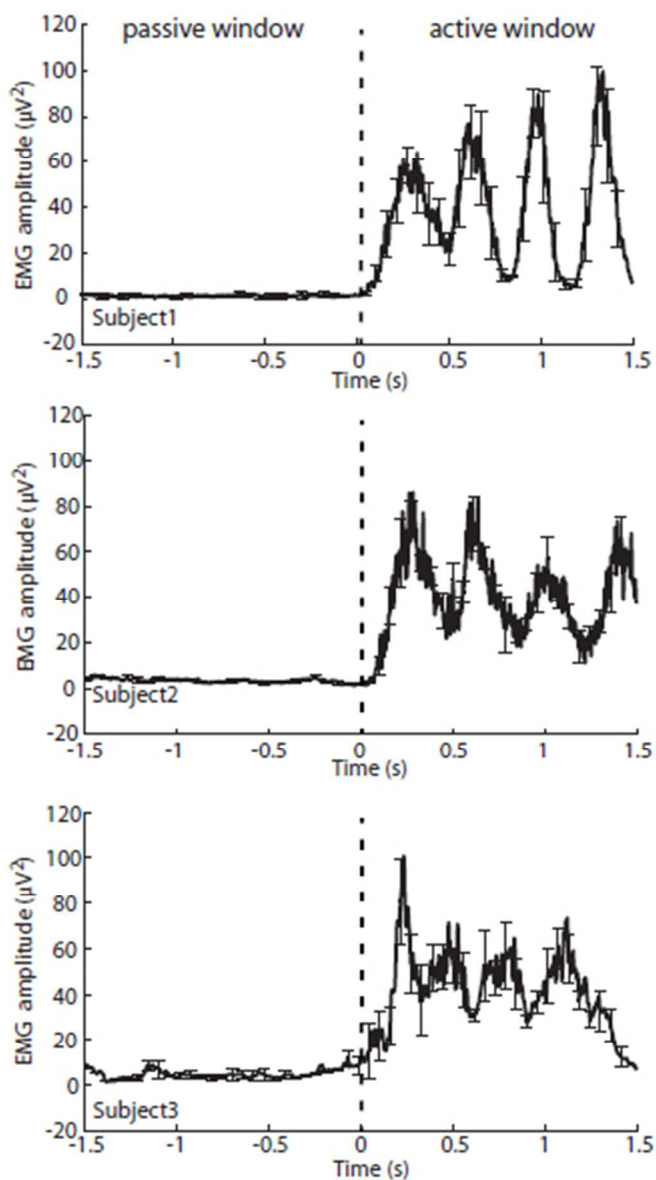
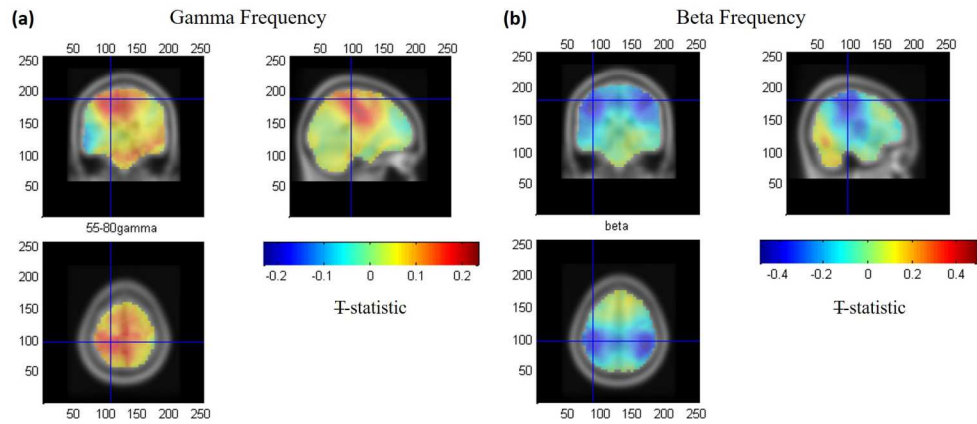


Figure 4. EMG activity recorded from the right FDI during the passive (-9 to -7.5s) and active (0-1.5s) time windows (here the time windows are concatenated together for visualisation purposes) from three representative subjects. The average timecourse across all trials and runs from a representative subject is shown. Onset of the first auditory cue occurred at 0s relative to index finger abduction movements. Error bars denote standard deviation across runs.

90x155mm (96 x 96 DPI)



22 Figure 5: Group average (N=10) T-statistic beamformer maps showing regions exhibiting power increases
23 and decreases in a) gamma- and b) beta-power, respectively, during the active window (0-1.5s) as
24 compared with the passive window (-9.5-7s). The crosshairs represent the group average of the individual
25 VE locations found in cM1 for the gamma (a) and beta (b) frequency activity.

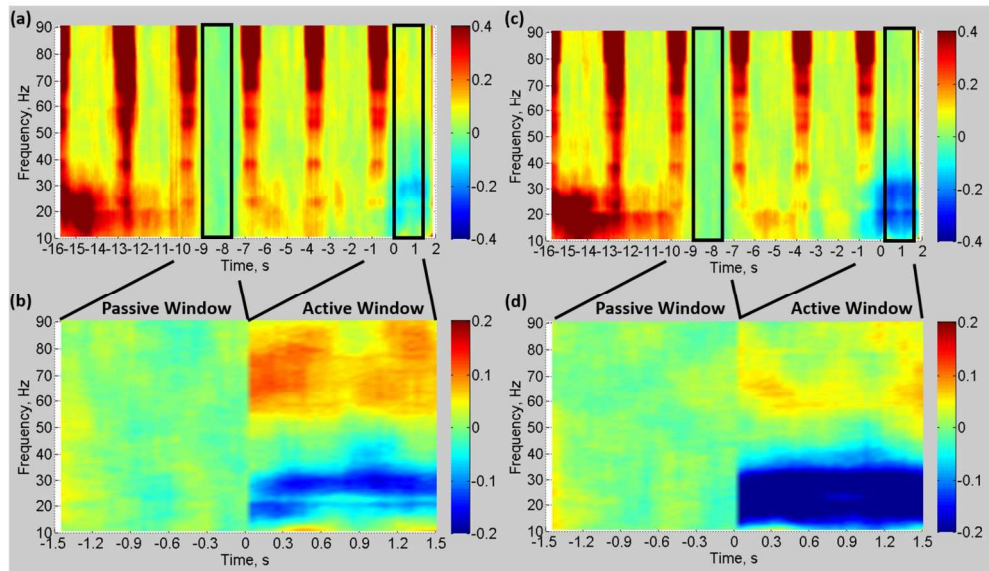
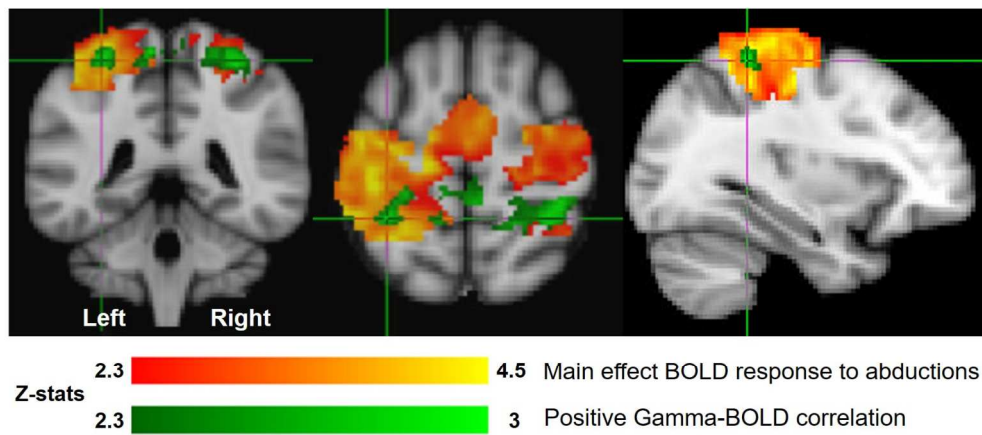


Figure 6: Group mean ($N=10$) time-frequency spectrograms demonstrating changes in the EEG signal power in cM1 relative to the passive window (-9 to -7.5s) for a&b) gamma ERS and c&d) beta ERD VE location. The passive window was located in an MR quiet period and before any anticipation of the stimulus. Time is displayed relative to the auditory cue onset. Spectrograms were calculated with frequency resolution of 2.5Hz with spectral smoothing of ± 10 Hz. a&c) show 18s whole-trial duration, note the residual GAs during fMRI acquisition periods. b&d) show the gamma and beta power responses during the active window (0 to 1.5s) where movement occurred, with the passive window data appended pre-stimulus for comparison. Colour bars denote the relative change in power from the average power during the passive window period (baseline measure) of the passive window for each frequency. See Figure S2 for absolute power changes of same time-frequency spectrograms.



22 Figure 7: Group average (N=10) fMRI mixed effects results. Positive correlation of BOLD signal to the boxcar
23 model of right index finger abduction movements (red-yellow) and areas of positive gamma-BOLD
24 correlation (green). All correlations are cluster corrected with $p < 0.05$, masked with motor cortex. The
25 crosshairs represent the peak positive gamma-BOLD correlation in cM1 (at [-32, -42, 60] mm).
26
27
28
29
30
31
32
33
34
35
36
37
38
39
40
41
42
43
44
45
46
47
48
49
50
51
52
53
54
55
56
57
58
59
60

Multiband Factor	Slice acquisition spacing	tSNR
1	Equidistant	74 ± 40
2	Equidistant	72 ± 39
2	Sparse	67 ± 37
3	Equidistant	68 ± 37
3	Sparse	74 ± 38

Table 1. Mean temporal SNR (tSNR) (\pm standard deviation) calculated over grey matter across 3 participants during five MR sequences: MB: 1-3; acquisition type = equidistant or sparse. All other parameters were constant: TR/TE=3060/40ms, SENSE=2, slices=36, FA=79°, Volumes=41.